MOLECULAR AND CELLULAR BIOLOGY, July 2007, p. 4844–4862 Vol. 27, No. 13
0270-7306/07/$08.00+0 doi:10.1128/MCB.02141-06

Sequential Activation of Poly(ADP-Ribose) Polymerase 1, Calpains, and Bax Is Essential in Apoptosis-Inducing Factor-Mediated Programmed Necrosis▽

Rana S. Moubarak,[1] Victor J. Yuste,[1] Cédric Artus,[1] Aïda Bouharrour,[1] Peter A. Greer,[2] Josiane Menissier-de Murcia,[3] and Santos A. Susin[1]*

Apoptose et Système Immunitaire, CNRS-URA 1961, Institut Pasteur, Paris, France[1]; Queen's Cancer Research Institute, Department of Pathology and Molecular Medicine, Queen's University, Kingston, Ontario, Canada[2]; and Département Intégrité du génôme CNRS-UMR 7175, Ecole Supérieure de Biotechnologie de Strasbourg, Illkirch, France[3]

Received 15 November 2006/Returned for modification 30 January 2007/Accepted 16 April 2007

Alkylating DNA damage induces a necrotic type of programmed cell death through the poly(ADP-ribose) polymerases (PARP) and *a*poptosis-*i*nducing *f*actor (AIF). Following PARP activation, AIF is released from mitochondria and translocates to the nucleus, where it causes chromatin condensation and DNA fragmentation. By employing a large panel of gene knockout cells, we identified and describe here two essential molecular links between PARP and AIF: calpains and Bax. Alkylating DNA damage initiated a p53-independent form of death involving PARP-1 but not PARP-2. Once activated, PARP-1 mediated mitochondrial AIF release and necrosis through a mechanism requiring calpains but not cathepsins or caspases. Importantly, single ablation of the proapoptotic Bcl-2 family member *Bax*, but not *Bak*, prevented both AIF release and alkylating DNA damage-induced death. Thus, Bax is indispensable for this type of necrosis. Our data also revealed that Bcl-2 regulates *N*-methyl-*N*′-nitro-*N*′-nitrosoguanidine-induced necrosis. Finally, we established the molecular ordering of PARP-1, calpains, Bax, and AIF activation, and we showed that AIF downregulation confers resistance to alkylating DNA damage-induced necrosis. Our data shed new light on the mechanisms regulating AIF-dependent necrosis and support the notion that, like apoptosis, necrosis could be a highly regulated cell death program.

Cellular changes leading to inhibition of programmed cell death (PCD) play an essential role in tumor development (90). The elucidation of cell death pathways is thus an important area of study that may provide insights into the causes of drug resistance, thereby facilitating the development of novel anticancer therapies. In the last decade, the study of PCD has predominantly focused on apoptosis. However, PCD can be divided into at least three different categories: apoptosis, autophagy, and necrosis (21). Apoptosis is characterized by cellular shrinkage, chromatin condensation, and DNA degradation, and is mediated by caspases (32). Autophagy is characterized by the engulfment of cellular organelles, such as mitochondria and endoplasmic reticulum, by cytoplasmic vesicles. Necrosis has often been considered a passive process lacking any signaling event. However, necrosis could also occur in a controlled fashion (4, 6, 7, 9, 33, 47, 48, 59, 75, 89). Thus, knowledge of the molecular mechanisms regulating necrosis could open the way to novel therapeutic approaches. On the one hand, analysis of the necrotic pathway may provide new options to destroy apoptosis-resistant tumor cells. On the other hand, a combination of therapies based on apoptosis mediators (e.g., caspases) and alternative therapies based on necrosis death effectors could offer a more effective approach.

* Corresponding author. Mailing address: Apoptose et Système Immunitaire, CNRS-URA 1961, Institut Pasteur, 25 Rue du Dr. Roux, 75015 Paris, France. Phone: 33 1 40 61 31 84. Fax: 33 1 40 61 31 86. E-mail: susin@pasteur.fr.

▽ Published ahead of print on 30 April 2007.

Alkylating agents, like the nitrosourea *N*-methyl-*N*′-nitro-*N*′-nitrosoguanidine (MNNG), kill apoptotic-resistant cells (88). They act by covalently modifying bases in the DNA, which results in massive production of DNA strand breaks and the induction of PCD. This type of death is controlled by the poly(ADP-ribose) polymerases (PARP), mainly represented by PARP-1 (113 kDa) and PARP-2 (63 kDa) (28, 85). The activation of PARP results in poly(ADP-ribosyl)ation of key DNA repair proteins at the expense of NAD^+, which is cleaved into ADP-ribose and nicotinamide. When DNA damage is limited (e.g., by MNNG treatment at 0.5 to 10 μM), this physiological machinery, which normally plays homeostatic protective and regulatory roles, could repair the injury (28, 63). If DNA breaks are repaired, the damaged cells survive and the cellular NAD^+ levels are restored by recycling nicotinamide with two ATP molecules. If DNA repair is not completely achieved, the cells undergo apoptosis by a caspase-dependent mechanism. When DNA damage is extensive (e.g., MNNG treatment at 100 to 500 μM), cells cannot repair the injury. In this case, disproportionate activation of PARP depletes the cellular pools of NAD^+ and ATP, driving the cell to a necrotic type of PCD (28, 63). Therefore, nitrosoureas could induce apoptosis or necrosis, depending on the level of the DNA damage produced. In any case, these agents join a growing list of possible therapeutics that can kill cancer cells by inducing necrosis, such as cisplatin (56) or β-lapachone (51).

Does necrosis induced by MNNG represent a programmed process? A strong link between PARP activation, release of

the proapoptotic protein *a*poptosis-*i*nducing *f*actor (AIF) from mitochondria, and PCD associated with MNNG damage has been reported. In neuronal and cervical carcinoma cells, MNNG-induced death has been found to be PARP dependent but caspase independent (82, 85). PARP chemical inhibitors, PARP-1 genetic ablation, or neutralizing anti-AIF antibodies inhibited MNNG-induced death (83, 85). Moreover, in DNA damage-induced PCD, AIF is released from mitochondria by a mechanism implicating PAR polymers (84), mitochondrial permeability transition (1), reactive oxygen species production (35), or RIP1/TRAF2-mediated Jun N-terminal protein kinase 1 activation (83). Therefore, it seems that PARP controls alkylating DNA damage-induced necrosis through the release of AIF from mitochondria.

AIF is a bifunctional NADH oxidase involved in mitochondrial respiration and caspase-independent apoptosis (69, 74). These two activities can be dissociated (8, 17, 18). Indeed, AIF plays a prosurvival role through its redox activity in mitochondria, but a lethal role upon its translocation to the nucleus. Once in the nucleus, AIF causes partial chromatin condensation and DNA fragmentation (69). This apoptogenic function of AIF is essential in some relevant experimental models of cell death (11–13, 23, 29, 35, 39, 40, 44, 49, 52, 55, 57, 77, 78, 85, 87). To be released from mitochondria, AIF needs to be cleaved into tAIF by calpain or cathepsins (50, 54, 86). Calpains are calcium-dependent proteases that are strongly implicated in PCD (53). The two ubiquitously expressed forms of calpain, μ- and m-calpain, require the *capn4*-encoded regulatory subunit for activity, and *capn4* knockout cells display resistance to endoplasmic reticulum-induced PCD (72). The lysosomal cathepsins have also been implicated in apoptosis and necrosis upon the loss of lysosomal membrane integrity (89).

Altogether, these findings emphasize the complexity of intracellular events triggering alkylating DNA damage-induced death. However, key questions remain to be addressed: How does the nuclear PARP activation trigger mitochondrial AIF release? Are calpains and/or cathepsins implicated in such release? Is the Bcl-2 family of proteins, which controls AIF release in apoptotic conditions (71), also implicated in the release of AIF during necrosis? Does AIF knockdown inhibit necrosis? The aim of the present work was to examine these issues by using a panel of gene-knockout murine embryonic fibroblasts (MEFs). This approach has elucidated a novel p53-independent death pathway that sequentially involves PARP-1, calpains, Bax, and AIF.

MATERIALS AND METHODS

Cell culture and cell death induction and inhibition. Cells were cultured in Dulbecco's modified Eagle's medium supplemented with 10% fetal calf serum, 2 mM L-glutamine, and 100 U/ml penicillin/streptomycin (Invitrogen) and maintained at 37°C in a 5% CO_2 atmosphere. *Bax*$^{-/-}$ and *Bak*$^{-/-}$ MEFs were provided by S. J. Korsmeyer (Dana-Farber Cancer Institute) and *Cathepsin L*$^{-/-}$ and *Cathepsin B*$^{-/-}$ MEFs by A. Rudensky (Howard Hughes Medical Institute). *PARP-1*$^{-/-}$, *PARP-2*$^{-/-}$, *p53*$^{-/-}$, and *Capn4*$^{-/-}$ MEFs were previously described (10, 42, 72). Wild-type (WT) cells from each lineage were used as controls. The genotypes of all cells were confirmed by immunoblotting.

To induce death, cells were treated with staurosporine (STS) (1 μM; 12 h), H_2O_2 (10 mM; 3 h), or MNNG (0.5 mM). For experiments with MNNG, the treatment medium was replaced after 15 min of incubation with fresh medium devoid of MNNG, and the cells (75 to 80% confluence) were cultured for the indicated times. Alternatively, cells were preincubated (1 h) with DHIQ (300 μM; Calbiochem), oligomycin (6 μM), Q-VD–OPh (QVD; 10 μM), z-VAD–fmk, Boc-D-fmk (BAF), z-VDVAD–fmk, z-DEVD–fmk, z-VEID–fmk, z-IETD–fmk, or z-LEHD–fmk (100 μM; MP Biomedicals) before MNNG treatment. In a separate set of experiments, MEFs were cultured during the 48 h before MNNG treatment in DMEM without glucose (Invitrogen) supplemented with 10% fetal calf serum and 100 U/ml penicillin-streptomycin.

Flow cytometry and necrosis quantification. We used annexin V-fluorescein isothiocyanate (FITC) (0.1 μg/ml) for the assessment of phosphatidylserine (PS) exposure, propidium iodide (PI; 0.5 μg/ml) for cell viability analysis, and tetramethylrhodamine ethyl ester (TMRE; 20 nM) for the quantification of mitochondrial transmembrane potential ($\Delta\Psi_m$). Cell death was recorded in a FACSCalibur cytofluorimeter (BD Biosciences). Lactate dehydrogenase (LDH) release was assessed with a CytoTox-ONE membrane integrity kit (Promega) in a Fluoroskan ascent fluorimeter (ThermoLab Systems).

DNA electrophoresis. Oligonucleosomal DNA fragmentation was detected by agarose gel electrophoresis as described elsewhere (58).

Determination of ATP content. Cells treated as indicated were lysed, and the total ATP content was assessed with a luciferin-luciferase kit from Sigma. Luminescence was measured in a Berthold LB96V MicroLumat plus. The ATP content is expressed in arbitrary units relative to the number of cells analyzed. The ATP quantified in control cells is referred to as 100%.

tAIF recombinant protein. tAIF mouse recombinant protein was produced as described elsewhere (86).

Terminal deoxynucleotidyltransferase-mediated dUTP-biotin nick end labeling (TUNEL) assay and cell-free system. The detection of 3′-OH DNA breaks was performed as described previously (87). Alternatively, cells were costained with Hoechst 33342, examined in a Nikon Eclipse TE2000-U microscope, and analyzed using Nikon ACT-1 software.

A cell-free system was made as reported (69). Briefly, MEF nuclei (10^3 nuclei/μl) were incubated in the presence of recombinant tAIF (5 μg/ml) for 90 min at 37°C. Nuclei were used for TUNEL and Hoechst 33342 labeling and examined by fluorescence microscopy as described above. Alternatively, nuclei were stained with PI (0.5 μg/ml) and analyzed by flow cytometry.

Protein extraction, cell fractionation, and immunoblotting. For whole protein extracts, 1×10^6 cells were lysed in buffer containing 20 mM Tris-HCl, pH 7.6, 150 mM NaCl, and 1% Triton X-100. For cytosolic purification, 2×10^6 cells were resuspended in buffer containing 220 mM mannitol, 70 mM sucrose, 50 mM HEPES-KOH (pH 7.2), 10 mM KCl, 5 mM EGTA, 2 mM $MgCl_2$, and 0.025% digitonine, and kept on ice for 5 min. Lysed cells were centrifuged (16,000 × *g*; 5 min; 4°C) and the supernatant was retained for the cytosolic fraction. The mitochondrial fractions were obtained by using a kit from Pierce and following the manufacturer's instructions. In vitro assays of AIF mitochondrial release upon atractyloside treatment were performed as described previously (86). For PAR detection, 1×10^6 cells were lysed as described previously (83). Twenty micrograms of protein was loaded on 4 to 12% NuPAGE or linear sodium dodecyl sulfate-polyacrylamide gel electrophoresis gels and transferred onto a nitrocellulose membrane. The membranes were probed with antibodies against Bax and caspase-9 (Upstate), Bcl-2 (BD Biosciences), PAR (clone LP98-10, Alexis), ICAD (inhibitor of caspase-activated DNase; Stressgen), α-spectrin (Chemicon), cleaved caspase-3 (BD Biosciences), Omi/HtrA2 (Alexis), Smac/DIABLO (ProSci Inc.), AIF, actin, μ-calpain (domain IV), or cytochrome *c*. In some experiments, equal loading was confirmed by staining the membrane with naphthol blue.

Cell transfection and siRNA assays. For Bcl-2 overexpression assays, cells were stably transfected either with pcDNA3.1 empty vector (Neo) or pcDNA3.1-Bcl-2. Bcl-2 overexpression was confirmed by immunoblotting, and the levels of cell death induced by MNNG were determined by using flow cytometry with double labeling with annexin V and PI. For AIF downregulation assays, WT MEFs were transfected in a Nucleofector system (Amaxa) with two specific small interfering RNA (siRNA) double-stranded oligonucleotides designed against mouse AIF (AIF siRNA I, 5′-GCATGCTTCTATGATATAA-3′, and AIF siRNA II, 5′-CTGGCGGACTGGAAATAGA-3′). As a control, we used an siRNA against lamin A (control siRNA, 5′-CTGGACTTCCAGAAGAACA-3′). Seventy-two hours after the indicated siRNA transfection, PCD was induced by MNNG and the levels of cell death were determined by PI exclusion.

AIF and PAR immunofluorescence. Cells seeded on coverslips were fixed in methanol, incubated with an anti-AIF (raised against a peptide mapping at the C terminus of AIF [amino acids 593 to 613]; Sigma-Aldrich) (86) or an anti-PAR (clone 10H; Alexis) antibody (15), and detected by anti-rabbit immunoglobulin G (IgG) conjugated with Alexa Fluor 488 (Invitrogen). Before being assessed, the cells were stained with Hoechst 33342 and mounted, and the green and blue fluorescence was observed in a confocal microscope (LSM-510 Meta; Zeiss). The cellular distribution of AIF was analyzed by using LSM-510 3.2 software. The quantification of chromatin condensation by fluorescence microscopy was per-

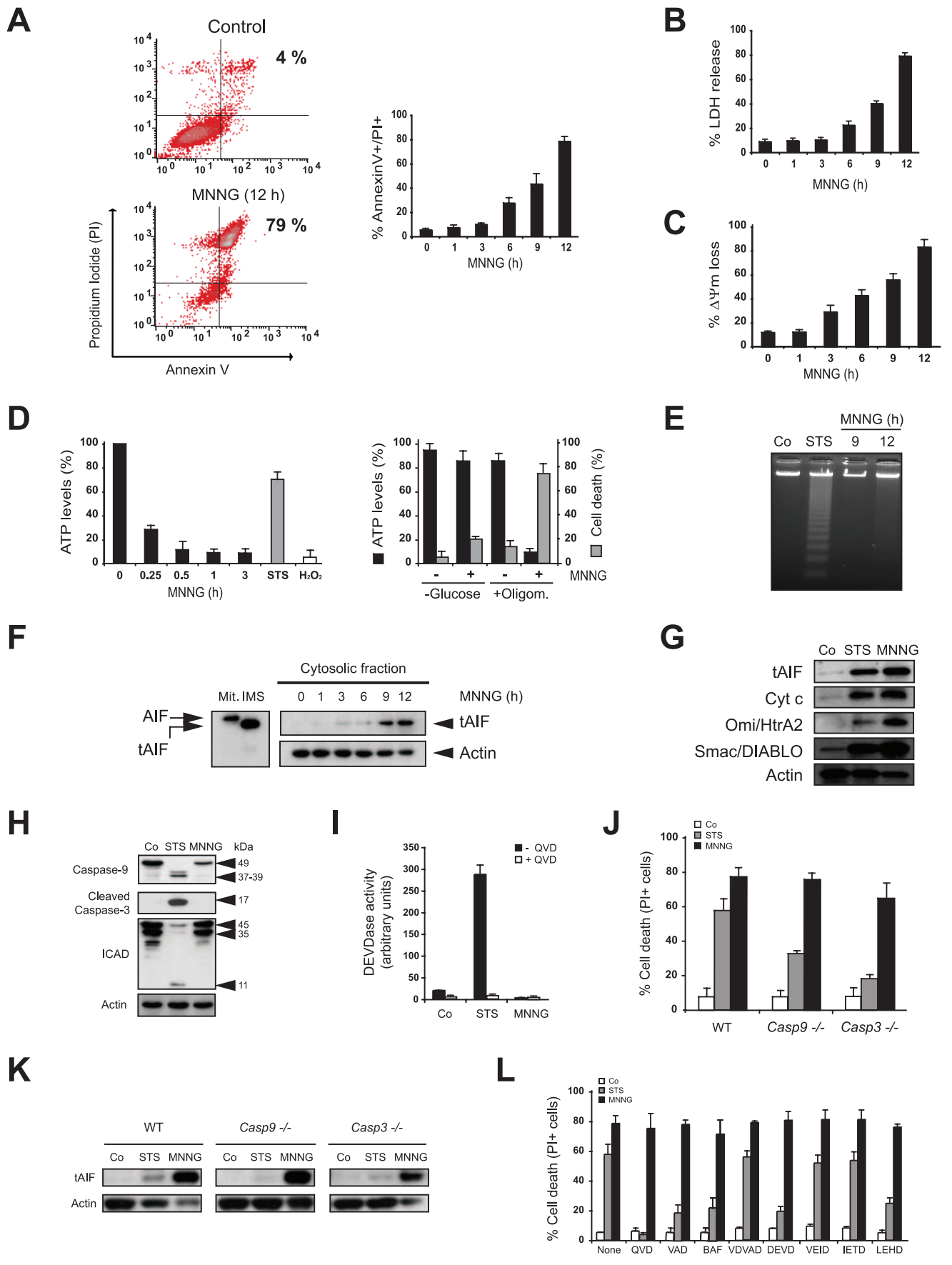
A
Control
4 %
MNNG (12 h)
79 %
Propidium Iodide (PI)
Annexin V
% AnnexinV+/PI+
MNNG (h)
B
% LDH release
MNNG (h)
C
% ΔΨm loss
MNNG (h)
D
ATP levels (%)
MNNG (h)
0 0.25 0.5 1 3 STS H2O2
ATP levels (%)
Cell death (%)
-Glucose +Oligom.
MNNG
E
MNNG (h)
Co STS 9 12
F
Cytosolic fraction
Mit. IMS
0 1 3 6 9 12
MNNG (h)
AIF
tAIF
tAIF
Actin
G
Co STS MNNG
tAIF
Cyt c
Omi/HtrA2
Smac/DIABLO
Actin
H
Co STS MNNG kDa
Caspase-9
49
37-39
Cleaved Caspase-3
17
ICAD
45
35
11
Actin
I
DEVDase activity (arbitrary units)
- QVD
+ QVD
Co STS MNNG
J
Co
STS
MNNG
% Cell death (PI+ cells)
WT Casp9 -/- Casp3 -/-
K
WT Casp9 -/- Casp3 -/-
Co STS MNNG
tAIF
Actin
L
Co
STS
MNNG
% Cell death (PI+ cells)
None QVD VAD BAF VDVAD DEVD VEID IETD LEHD

formed in blind testing by at least two investigators, on 100 cells for each data point, and was repeated at least three times in independent experiments.

Bax activation, redistribution, and transfection. For flow cytometry or immunofluorescence analysis, cells were fixed in 1% paraformaldehyde, permeabilized with 0.1% saponin (10 min), incubated with an antibody designed against the active form of Bax (clone 6A7; BD Biosciences) (1 h), and detected by an anti-mouse IgG conjugated with Alexa Fluor 488 (Invitrogen). The cells were either analyzed by cytofluorometry or stained with Hoechst 33342 for immunofluorescence assessment. Images were acquired with an Apotome-equipped Zeiss Axioplan (Axiocam MR; Zeiss) and examined with Axiovision software. For the assessment of Bax mitochondrial redistribution, cells were fixed as above, incubated with anti-Bax (Upstate) and anti-OxPhos complex IV subunit I (COX IV; Invitrogen) antibodies, and detected by anti-mouse and anti-rabbit IgG conjugated with Alexa Fluor (Invitrogen) according to standard procedures. Images were visualized in a Nikon Eclipse TE-2000-U fluorescent microscope, acquired with a Nikon digital DXM 1200 camera, and analyzed using Nikon ACT-1 software, version 2.2. For Bax immunoprecipitation, we used a method described elsewhere (27). After the immunoprecipitation, samples were loaded on a 15% acrylamide gel and analyzed by immunoblotting for Bax as described above. For determining the levels of transient Bax overexpression, MEFs were transfected in a Nucleofector system (Amaxa) with pcDNA3-Bax or pcDNA3 empty vector. Twelve hours after the indicated transfections, PCD was induced by MNNG and cell viability assessed by PI labeling.

Caspase activity. Cells treated as indicated above were lysed in caspase assay buffer containing 40 mM HEPES-NaOH, pH 7.2, 300 mM NaCl, 20 mM dithiothreitol, 10 mM EDTA, 2% Nonidet P-40, 20% sucrose, and 100 μM of *N*-acetyl-DEVD-AFC (7-amino-4-trifluoromethyl coumarin). The level of caspase activity was read in a fluorimeter.

Determination of total NAD^+ content. The NAD^+ concentrations were measured as described previously (88) in a Multiskan ascent spectrophotometer. The protein levels were determined by using a Bradford protein assay (Bio-Rad), and the NAD^+ contents were related to the protein levels.

Calpain activity. The calpain activities present in 30 μg of total cell lysates were determined by cleavage of the fluorescent substrate *N*-succinyl-LLVY-AMC (Calbiochem) and expressed as the difference between calcium-dependent and calcium-independent fluorescence. Calcium-dependent fluorescence was measured after 30 min of incubation at 37°C in buffer containing 63 mM imidazole-HCl, pH 7.3, 10 mM β-mercaptoethanol, and 5 mM $CaCl_2$. Calcium-independent fluorescence was measured under the same conditions but using buffer without $CaCl_2$ and containing 1 mM EDTA and 10 mM EGTA. The fluorescence was recorded in a Fluoroskan ascent fluorimeter. The levels of calpain activity in live cells were detected by using the cell-permeable calpain substrate Boc-Leu-Met-CMAC (Invitrogen). Cells spread on coverslides were incubated for 30 min with 50 μM of calpain substrate in Dulbecco's modified Eagle's medium. The cells were then treated for 1 h with 0.5 mM of MNNG, observed in a Nikon Eclipse TE2000-U microscope, and analyzed using Nikon ACT-1 software, version 2.2.

Unless specified, reagents were from Sigma-Aldrich.

RESULTS

The DNA alkylating agent MNNG induces caspase-independent necrosis. To identify the type of cell death induced by alkylating DNA damage, we first examined the biochemical events induced by MNNG treatment in MEFs. As depicted in Fig. 1A, MNNG-induced death is a time-dependent process, with significant alterations observed as soon as 6 h after treatment and a maximum effect at 12 h. By measuring the level of LDH release, which only occurs in necrotic conditions, we determined that the cytotoxic process induced by MNNG is similar to necrosis (Fig. 1B). MNNG-treated cells underwent PS exposure, loss of cell viability, and $\Delta\Psi_m$ dissipation (Fig. 1A and C). In contrast, MNNG treatment was not coupled to oligonucleosomal DNA degradation (Fig. 1E) or signs of lysosomal permeabilization (data not shown). The cellular alterations observed after MNNG treatment are associated with a rapid drop in ATP levels (Fig. 1D) and mitochondrial release of tAIF (the cleaved form of AIF) (86), cytochrome *c*, Omi/HtrA2, or Smac/DIABLO to the cytosol (Fig. 1F and G). These results confirm that, as in apoptotic PCD (45), the different mitochondrial intermembrane space proteins are released during necrosis. Interestingly, ATP levels are maintained in cells cultured in the absence of glucose or upon treatment with the mitochondrial ATP synthase inhibitor oligomycin, indicating that the MEFs used either glycolysis or mitochondrial oxidative phosphorylation to maintain their

FIG. 1. MNNG-induced cell death is caspase-independent. (A) After the indicated time post-MNNG treatment, WT MEFs were stained with annexin V-FITC and PI, and the frequency of double-positive labeling was recorded and illustrated as a plot. The data presented in the bar chart are the means ± standard deviations (SDs) of the results of five independent experiments. In the cytometry panels, the percentages refer to the levels of double-positive staining. (B) At the indicated times, the level of extracellular LDH from MNNG-treated MEFs was assessed and expressed as a percentage of the total LDH released from Triton X-100-lysed cells. The data shown are the means ± SDs of the results ($n = 4$). (C) The cells were treated with MNNG for the indicated times and then labeled with TMRE and assessed for the loss of $\Delta\Psi_m$. The results shown are the means ± SDs of the results of three independent experiments. (D) Quantification of the intracellular ATP levels in WT MEFs treated with MNNG at the indicated times (left graph). Alternatively, the cells were cultured for 48 h in complete medium without glucose (−Glucose) or treated with oligomycin (+Oligom; 6 μM) for 30 min prior to MNNG treatment (1 h), and the ATP levels were determined (right graph). STS or H_2O_2 was used as an apoptotic or necrotic inducer, respectively. The basal ATP levels scored in control cells cultured in complete medium are referred to as 100%. The levels of cell death were measured by means of annexin V-FITC and PI staining in untreated cells (−) or cells treated with MNNG (+) for 9 h, as described in Materials and Methods. The data shown are the means ± SDs of the results ($n = 4$). (E) Assessment of oligonucleosomal DNA fragmentation in WT MEFs not treated (Co) or incubated with MNNG (9 and 12 h). STS (6 h) was used as a positive control. (F) Mitochondrial AIF (Mit) is cleaved into a lower-molecular-weight tAIF in the mitochondrial intermembrane space (IMS) upon atractyloside treatment. The cytosolic fractions recovered after MNNG treatment were blotted for AIF detection. As in isolated mitochondria, MNNG treatment induces both AIF cleavage into tAIF and time-dependent tAIF release to the cytosol. Actin was used as a loading control. (G) Cytosolic extracts from untreated (Co) or STS- or MNNG-treated (12 h) cells were tested for the release of cytochrome *c*, Omi/HtrA2, and Smac/DIABLO. The actin levels were analyzed as a loading control. (H) Total cell lysates from WT MEFs not treated (Co) or treated with STS or MNNG (12 h) were probed for the detection of caspase-9 or -3 or ICAD. Equal loading was confirmed by actin assessment. Molecular mass markers are on the right. (I) Fluorometric measurement of caspase-3 activities observed in cytosolic extracts obtained from WT MEFs not treated (Co) or treated with STS or MNNG (12 h) in the absence or presence of the pancaspase inhibitor QVD. The results shown are the means ± SDs of the results of three experiments. (J) WT, *Casp-9*$^{-/-}$, and *Casp-3*$^{-/-}$ MEFs were not treated (Co) or treated with STS or MNNG (12 h), and the levels of cell death were measured by PI staining. The data shown are the means ± SDs of the results ($n = 4$). (K) The levels of tAIF release were detected in cytosolic extracts purified from WT, *Casp-9*$^{-/-}$, and *Casp-3*$^{-/-}$ MEFs treated as described for panel J. Actin detection was used as a loading control. (L) Assessment of levels of cell death in WT MEFs preincubated with the pancaspase inhibitors QVD, z-VAD–fmk, or BAF or specific inhibitors of caspase-2 (z-VDVAD–fmk), -3 and -7 (z-DEVD–fmk), -6 (z-VEID–fmk), -8 and -10 (z-IETD–fmk), or -9 (z-LEHD–fmk) before the induction of cell death by STS or MNNG treatment (12 h). The results shown are the means ± SDs of the results of five independent experiments.

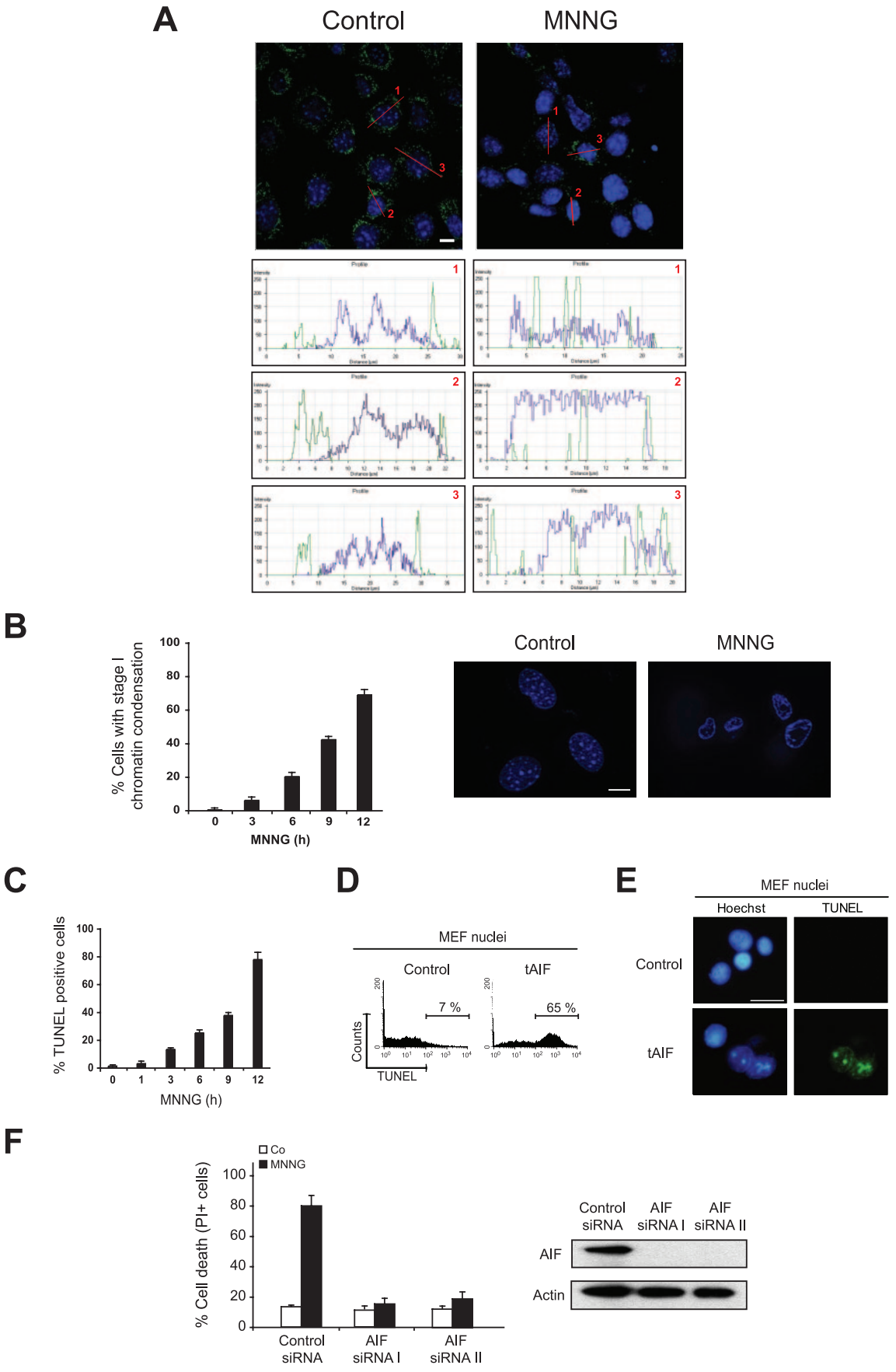
A
Control
MNNG
B
% Cells with stage I chromatin condensation
MNNG (h)
Control
MNNG
C
% TUNEL positive cells
MNNG (h)
D
MEF nuclei
Control
tAIF
7 %
65 %
Counts
TUNEL
E
MEF nuclei
Hoechst
TUNEL
Control
tAIF
F
Co
MNNG
% Cell death (PI+ cells)
Control siRNA
AIF siRNA I
AIF siRNA II
Control siRNA
AIF siRNA I
AIF siRNA II
AIF
Actin

metabolic status (Fig. 1D, right histogram). As an internal control, we verified that cells cultured in the absence of glucose and treated with oligomycin are unable to generate ATP (data not shown). Importantly, in MEFs, MNNG treatment induces necrosis only in cells using the glycolytic pathway (Fig. 1D).

We further explored the involvement of caspases in MNNG-mediated necrosis. First, we assessed the activation of two key players of caspase-dependent PCD: caspase-9 and caspase-3. These proteases are synthesized as inactive proenzymes of 49 and 32 kDa, respectively. After a caspase-dependent apoptotic insult, such as treatment with STS, caspase-9 and -3 are cleaved to yield the active p37/39 and p17 subunits of 37, 39, and 17 kDa, respectively. Immunoblot analysis demonstrated that, in contrast to the results from treatment with STS, caspase-9 and caspase-3 did not become activated even 12 h after MNNG treatment (Fig. 1H). This result demonstrated that MNNG-induced necrosis does not involve the activation of caspase-9 or caspase-3. Furthermore, in contrast to the results of STS treatment, caspase-3-dependent ICAD cleavage was not observed in MNNG-treated cells (Fig. 1H). Additional evidence that MNNG does not induce caspase-3 activity was seen in the results of a fluorogenic substrate-based assay (Fig. 1I). Finally, MNNG treatment of caspase-9 and caspase-3 knockout MEFs resulted in levels of cell death (Fig. 1J) and tAIF release from mitochondria (Fig. 1K) similar to those seen in WT cells. Together, these results show that MNNG-induced PCD is independent of caspase-9 and caspase-3.

On a broader scale, the caspase independence of the death process induced by MNNG was explored using a large panel of caspase inhibitors. We found that MNNG-induced PCD was not affected by the pancaspase inhibitors QVD, z-VAD, and BAF or by inhibitors of caspase-2, -3, -6, -7, -8, -9, or -10 (Fig. 1L).

Our data confirm that the caspase-independent PCD induced by MNNG treatment is similar to necrosis. The biochemical alterations observed after MNNG treatment linked PS exposure, loss of cell viability, $\Delta\Psi_m$ disruption, and ATP drop with the release of the cleaved form of AIF from mitochondria to the cytosol.

AIF redistributes from mitochondria to nucleus and controls MNNG-induced necrosis. During caspase-independent PCD, AIF translocates from mitochondria to the nucleus, where it causes a type of nuclear alteration, named stage I, characterized by rippled nuclear contours and partial chromatin condensation (68). Thus, we tested whether MNNG-induced AIF relocation provokes this nuclear hallmark in MEFs. In untreated cells, AIF was excluded from the nucleus and displayed a punctate mitochondrial localization pattern (Fig. 2A). However, after MNNG treatment, a portion of AIF was found within the nucleus, as determined by confocal and computerized image analysis (Fig. 2A). Kinetic studies established a correlation between necrosis (Fig. 1A, B, and C), mitochondrial translocation of tAIF (Fig. 1D), and the advancement of nuclear PCD (Fig. 2B). Interestingly, TUNEL assessment revealed that stage I of the chromatin condensation was accompanied by 3′-OH DNA breaks in MNNG-induced necrosis (Fig. 2C). We thus generated the mouse tAIF recombinant protein to investigate whether the 3′-OH DNA breaks observed in MNNG-treated MEFs could be directly caused by tAIF. This recombinant protein was added to highly purified MEF nuclei in a cell-free in vitro system, and the levels of nuclear 3′-OH DNA breaks were assessed by two independent methods: cytofluorometry, to quantify the nuclei presenting DNA breaks, and immunofluorescence, to visualize the levels of TUNEL positivity. In both systems, we observed that, in vitro, recombinant tAIF causes the same nuclear apoptogenic effects as those observed in MNNG-treated cells (Fig. 2C and 2E). Finally, using siRNA-mediated knockdown of AIF, we confirmed that a reduction of AIF expression prevented MNNG-induced PCD (Fig. 2F). These results demonstrated that MNNG treatment induced necrosis through a direct effect of tAIF on the nucleus.

MNNG-induced AIF release and necrosis is a PARP-1-dependent and PARP-2/p53-independent process. We next investigated the mechanisms controlling AIF release in this type of cell death. The PARP family of proteins, mainly represented by PARP-1 and PARP-2, are regulators of the necrosis pathway and, depending on the cell death inducer, can promote AIF mitochondrial release in a p53-dependent or p53-independent manner (16, 36). Here we observed that, as in WT cells, MNNG triggered necrosis in *PARP-2*$^{-/-}$ or *p53*$^{-/-}$ cells, but not in *PARP-1*$^{-/-}$ MEFs (Fig. 3A). Therefore, MNNG-induced PCD was selectively regulated by PARP-1. It is important to note that, in the absence of PARP-1 expression, only a residual PAR activity was detected early after DNA damage-mediated cell death (Fig. 3B). Consequently, WT, *PARP-2*$^{-/-}$,

FIG. 2. The MNNG-induced PCD results correlate with the AIF relocalization from mitochondria to the nucleus and the levels of 3′-OH DNA breaks. (A) WT MEFs were not treated (Control) or treated with MNNG (6 h), immunostained for AIF detection (green), and examined by confocal microscopy. Hoechst 33342 (blue) was used to visualize the nuclei. The graphs represent the green/blue fluorescence distribution detected in the indicated cell sections. This experiment was repeated four times, yielding similar results. Bar, 10 μm. (B) WT MEFs were treated with MNNG for the indicated times and stained with Hoechst 33342 to visualize the nuclei. The numbers of cells presenting stage I of chromatin condensation were quantified and plotted as percentages of total cells (left panel). The data shown are the means ± standard deviations (SDs) of the results ($n = 5$). Representative nuclei from untreated (Control) or MNNG-treated (9 h) cells are shown (right panel). Bar, 10 μm. (C) At the indicated times after MNNG treatment, WT MEFs were stained for the detection of 3′-OH DNA breaks and analyzed by flow cytometry. The data shown are the means ± SDs of the results of five independent experiments. (D) Purified MEF nuclei were incubated in the absence (Control) or presence of mouse recombinant tAIF (7 μg/ml) and the presence of 3′-OH DNA breaks was determined by cytofluorometry. (E) In an experiment similar to that described for panel D, nuclei were stained with Hoechst 33342 and the levels of blue and green (TUNEL-positive) fluorescence were visualized. Representative microphotographs from untreated (Control) or tAIF-treated nuclei are shown. Bar, 20 μm. (F) WT MEFs were transfected with an siRNA against lamin A (Control siRNA) or two siRNAs against mouse AIF (AIF siRNAs I and II). Seventy-two hours after the indicated transfections, the MEFs were treated with MNNG or not treated (Co), and then the levels of cell death were assessed by flow cytometry by means of PI staining (left panel). The data shown are the means ± SDs of the results ($n = 5$). Immunoblotting analysis demonstrated the efficacy of siRNA-mediated AIF knockdown (right panel). Equal loading was confirmed by actin detection.

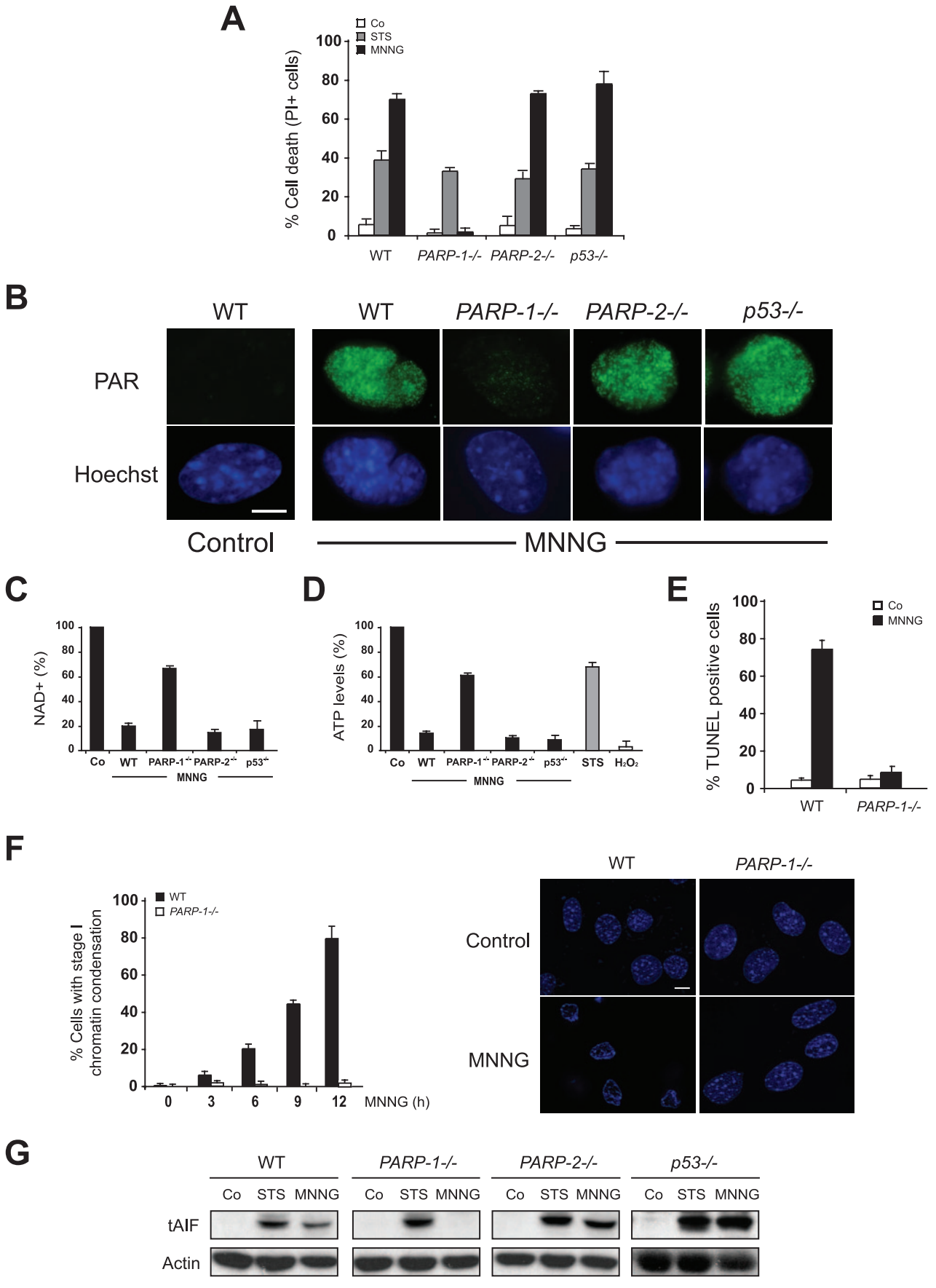
A
Co
STS
MNNG
% Cell death (PI+ cells)
100
80
60
40
20
0
WT
PARP-1-/-
PARP-2-/-
p53-/-
B
WT
WT
PARP-1-/-
PARP-2-/-
p53-/-
PAR
Hoechst
Control
MNNG
C
NAD+ (%)
100
80
60
40
20
0
Co
WT
PARP-1-/-
PARP-2-/-
p53-/-
MNNG
D
ATP levels (%)
100
80
60
40
20
0
Co
WT
PARP-1-/-
PARP-2-/-
p53-/-
STS
H2O2
MNNG
E
% TUNEL positive cells
100
80
60
40
20
0
Co
MNNG
WT
PARP-1-/-
F
WT
PARP-1-/-
% Cells with stage I chromatin condensation
100
80
60
40
20
0
0
3
6
9
12
MNNG (h)
WT
PARP-1-/-
Control
MNNG
G
WT
PARP-1-/-
PARP-2-/-
p53-/-
Co
STS
MNNG
tAIF
Actin

or *p53*$^{-/-}$ MEFs exhibited an important reduction in cellular NAD^+ and ATP levels, whereas in *PARP-1*$^{-/-}$ MEFs, NAD^+ and ATP levels are maintained near the control values (Fig. 3C and D). The resistance to MNNG displayed by *PARP-1*$^{-/-}$ MEFs correlates with the negative TUNEL labeling (Fig. 3E), the lack of generation of stage I of chromatin condensation (Fig. 3F), and the absence of tAIF release from mitochondria (Fig. 3G). These data indicated that MNNG induced tAIF release and necrosis in a PARP-1-dependent and a PARP-2/p53-independent manner.

Calpains regulate AIF release and MNNG-mediated necrosis. We next focused on the characterization of the molecular pathway regulating the PARP-1-dependent mitochondrial AIF release. AIF needs to be processed by calpains or cathepsin B, L, or S in the intermembrane space of mitochondria to yield a proapoptotic protein which is released to the cytosol (86). We therefore tested whether these proteases were implicated in MNNG-induced AIF release and necrosis. To address this issue, we used a panel of knockout MEFs for cathepsin B (*Cath B*$^{-/-}$), cathepsin L (*Cath L*$^{-/-}$) or the regulatory subunit of μ- and m-calpain (*Capn4*$^{-/-}$). Of note, MEFs do not express detectable levels of cathepsin S (data not shown). In *Cath B*$^{-/-}$ or *Cath L*$^{-/-}$ MEFs, both mitochondrial AIF release and MNNG-induced necrosis remained unaffected (Fig. 4A and B). In contrast, MNNG-induced AIF release and necrosis were completely abolished in *Capn4*$^{-/-}$ MEFs (Fig. 4C and D). Moreover, as expected from the absence of tAIF in extramitochondrial compartments in MNNG-treated *Capn4*$^{-/-}$ MEFs, the results of TUNEL labeling were also negative (Fig. 4E). As an internal control for calpain activation in MNNG-treated cells, we used a cell-permeable fluorescent calpain substrate, which reports calpain activity in live cells. This approach showed that MNNG treatment induced rapid calpain activation in WT, but not in *Capn4*$^{-/-}$, MEFs (Fig. 4F). These results were further corroborated by the results of a fluorescence assay (Fig. 4G) and immunoblotting (Fig. 4H). Hence, calpains were activated early after MNNG treatment, and the ensuing AIF release and cell death correlated with the levels of calpains but not of cathepsins.

Calpains act downstream of PARP-1 in MNNG-induced death. To gain insights into the molecular ordering of PARP-1 and calpains in MNNG-induced necrosis, we first tested whether PARP-1 was activated in *Capn4*$^{-/-}$ MEFs. As indicated above, activation of PARP-1 results in poly(ADP-ribosyl)ation at the expense of NAD^+. Thus, PARP-1 activation is detected biochemically by the inverse relationship existing between the cellular levels of PAR and NAD^+. As shown by the formation of PAR polymers, PARP-1 was equally activated in WT and *Capn4*$^{-/-}$ MEFs (Fig. 5A), demonstrating that PARP-1 is activated even in the absence of calpains. In agreement with this, MNNG treatment caused a rapid decrease in NAD^+ cellular levels in both WT and *Capn4*$^{-/-}$ MEFs. The specificity of the PARP-dependent NAD^+ loss associated with MNNG treatment was confirmed by using a pharmacological PARP inhibitor, DHIQ (Fig. 5B). Together, these data showed that PARP-1 activation was calpain-independent during MNNG-induced death, suggesting that calpain activity is placed downstream from PARP-1 activation in this process.

To confirm this hypothesis, we used a biochemical approach to determine whether calpains were activated in *PARP-1*$^{-/-}$ cells after MNNG treatment. First, we immunodetected the cleaved forms of the calpain substrate spectrin. Spectrin is a 240-kDa protein cleaved by calpains and caspase-3 in cell death conditions. While both calpains and caspase-3 produce fragments of 150 kDa, these proteases also produce distinct breakdown products: a 147-kDa fragment specifically generated by calpains and a 120-kDa fragment generated by caspase-3 (30). As depicted in Fig. 5C, WT MEFs treated with MNNG showed the 150-kDa common breakdown product and the 147-kDa calpain-specific product but not the 120-kDa caspase-3-specific product. However, spectrin was not cleaved in MNNG-treated *PARP-1*$^{-/-}$ MEFs, indicating that calpains were inactive in the absence of PARP-1. As a positive control for caspase-3-mediated spectrin cleavage, we demonstrated that WT and *PARP-1*$^{-/-}$ cells treated with the caspase-dependent apoptosis inductor STS displayed the 120-kDa spectrin breakdown product (Fig. 5C). As a control for calpain-mediated spectrin cleavage, we corroborated that this protein was not cleaved in *Capn4*$^{-/-}$ MEFs after alkylating DNA damage treatment (Fig. 5C). Finally, the blockade of calpain activation in MNNG-treated *PARP-1*$^{-/-}$ MEFs was confirmed by using a fluorescent substrate (Fig. 5D). Together, these results revealed that PARP-1 controls calpain activation during alkylating DNA damage-induced necrosis.

FIG. 3. Necrosis induced by DNA alkylation is PARP-1 dependent and PARP-2/p53 independent. (A) WT, *PARP-1*$^{-/-}$, *PARP-2*$^{-/-}$, and *p53*$^{-/-}$ MEFs were not treated (Co) or treated with STS or MNNG (12 h), and the levels of cell death were measured by analysis of PI staining. The results shown are the means ± standard deviations (SDs) of the results of three independent experiments. (B) WT, *PARP-1*$^{-/-}$, *PARP-2*$^{-/-}$, and *p53*$^{-/-}$ MEFs were not treated (Control) or treated with MNNG (5 min), immunostained for PAR detection (green), and visualized by confocal microscopy. Hoechst 33342 (blue) was used to visualize the nuclei. Representative micrographs of each cell type are shown. This experiment was repeated four times, yielding similar results. Bar, 10 μm. (C) WT, *PARP-1*$^{-/-}$, *PARP-2*$^{-/-}$, and *p53*$^{-/-}$ cells were treated with MNNG (15 min) and analyzed by measuring absorbance at 570 nm to assess the total NAD^+ levels. The concentrations of NAD^+ were normalized to those from untreated cells (Co). The results shown are the means ± SDs of the results of four experiments. (D) Quantification of the intracellular ATP levels in WT, *PARP-1*$^{-/-}$, *PARP-2*$^{-/-}$, and *p53*$^{-/-}$ MEFs treated with MNNG (15 min). STS or H_2O_2 was used as an apoptotic or necrotic inducer, respectively. The basal level of ATP scored in the control cells (Co) is referred to as 100%. The data shown are the means ± SDs of the results of five independent experiments. (E) WT and *PARP-1*$^{-/-}$ MEFs were not treated (Co) or treated with MNNG (12 h), stained for the detection of 3′-OH DNA breaks, and analyzed by flow cytometry. The data shown are the means ± SDs of the results ($n = 6$). (F) WT and *PARP-1*$^{-/-}$ MEFs were treated with MNNG for the indicated times and stained with Hoechst 33342 to visualize the nuclei. Representative nuclei of untreated cells (Control) or cells treated with MNNG (9 h) are shown (right panel). Bar, 10 μm. The numbers of cells presenting stage I of chromatin condensation were quantified and plotted as percentages of total cells (left panel). The data shown are the means ± SDs of the results ($n = 5$). (G) tAIF release was detected in cytosolic extracts purified from WT, *PARP-1*$^{-/-}$, *PARP-2*$^{-/-}$, and *p53*$^{-/-}$ MEFs treated as described for panel A. Actin detection was used as a loading control.

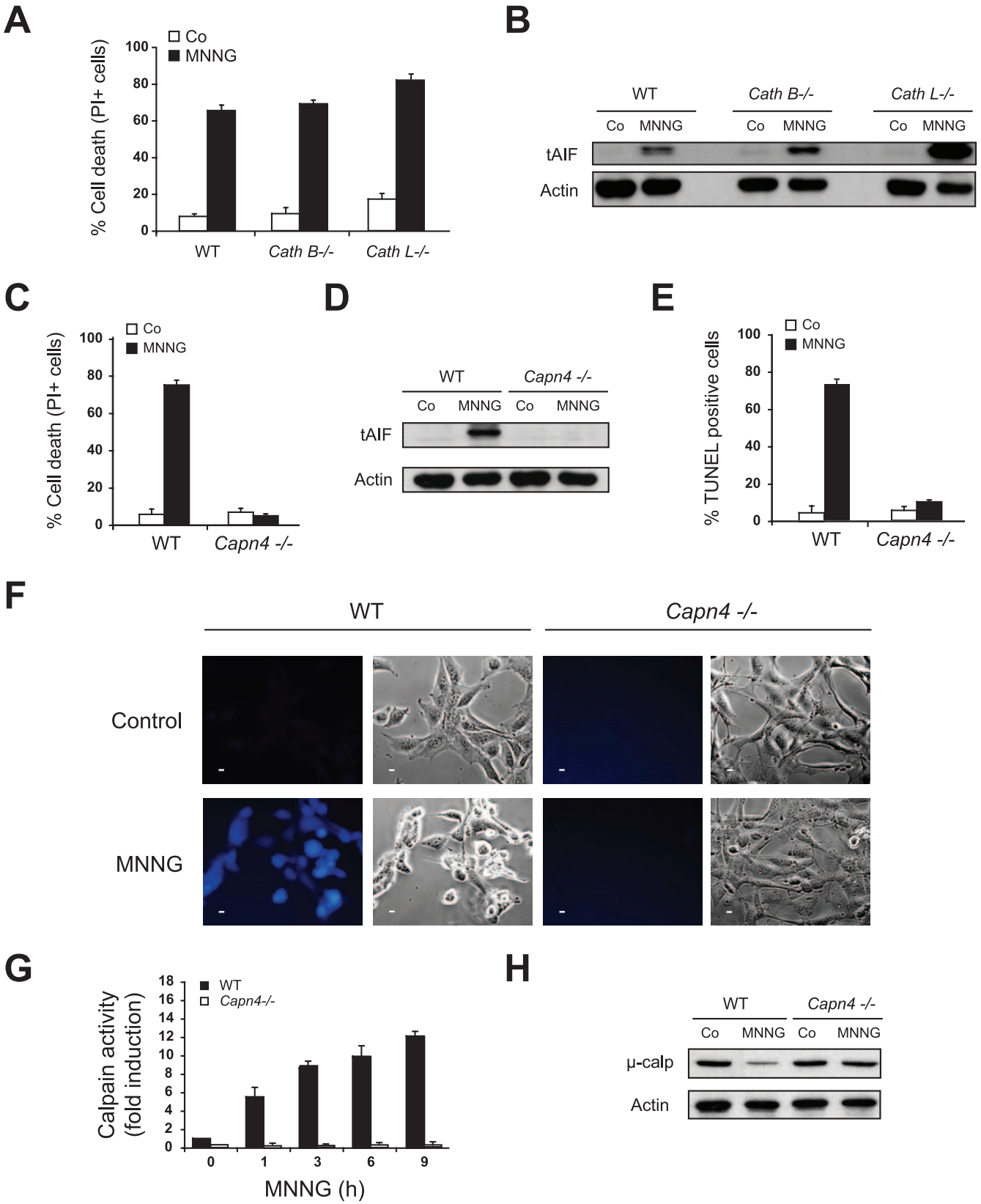

FIG. 4. Calpains, but not cathepsins, regulate mitochondrial AIF release during MNNG-induced necrosis. (A) WT, *Cath B*$^{-/-}$, and *Cath L*$^{-/-}$ MEFs were not treated (Co) or treated with MNNG (12 h), and the levels of cell death were measured by PI staining. The results shown are the means ± standard deviations (SDs) of the results of four independent experiments. (B) The levels of tAIF release were detected in cytosolic extracts purified from WT, *Cath B*$^{-/-}$, and *Cath L*$^{-/-}$ MEFs treated as described for panel A. The actin levels were assessed as a loading control.

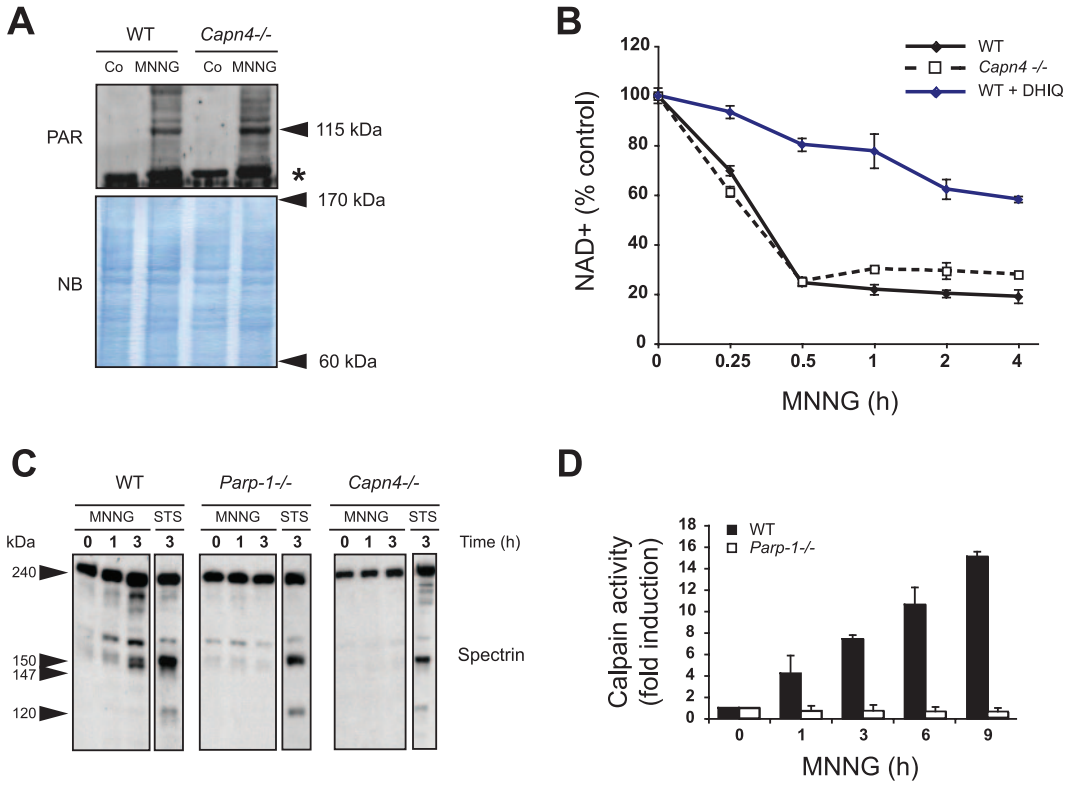

FIG. 5. PARP-1 is activated upstream of calpains during MNNG-induced cell death. (A) PAR detection by immunoblotting (115-kDa band) in total extracts from WT and *Capn4*$^{-/-}$ MEFs not treated (Co) or treated with MNNG (15 min). Molecular masses are shown on the right. The asterisk marks a nonspecific band. The membrane was stained with naphthol blue (NB) to assess protein loading. (B) WT and *Capn4*$^{-/-}$ MEFs were preincubated, or not, with the PARP inhibitor DHIQ and then treated with MNNG for the indicated times and analyzed by measuring absorbance at 570 nm to assess total NAD^+ levels. The concentrations of NAD^+ were normalized to those from untreated cells. The data shown are the means ± standard deviations of the results ($n = 5$) (C) Spectrin immunoblotting analysis was performed on total cell lysates from WT, *PARP-1*$^{-/-}$, and *Capn4*$^{-/-}$ MEFs treated with MNNG or STS for the indicated times. Full-length spectrin (240 kDa) and both the calpain-dependent (150 and 147 kDa) and caspase-3-dependent (150 and 120 kDa) fragments are indicated. (D) Fluorometric analysis of the calpain activity observed in extracts obtained from WT and *PARP-1*$^{-/-}$ MEFs treated with MNNG for the indicated times. The basal level of calpain activity observed in untreated cells is referred to as 1 unit. The data shown are the means ± standard deviations of the results ($n = 4$).

Bax, but not Bak, is necessary for MNNG-induced AIF release and necrosis. Next, we analyzed how the mitochondrial outer membrane became permeable to AIF after MNNG treatment. For this purpose, we studied the involvement of the Bcl-2 family of proteins in this process. Mitochondrial outer membrane permeabilization (MOMP) arises from a pore formed by proapoptotic Bcl-2 family members such as Bax and Bak, either alone or in combination with other proteins, like ANT (adenine nucleotide translocase) or VDAC (voltage-dependent anion channel) (37). Thus, we assessed whether Bak or Bax regulates MNNG-mediated AIF release and PCD. *Bak*$^{-/-}$ and WT MEFs displayed comparable MNNG-induced cell death responses. However, *Bax*$^{-/-}$ MEFs were largely resistant to MNNG treatment (Fig. 6A and B). In contrast, WT, *Bak*$^{-/-}$, and *Bax*$^{-/-}$ cells treated with the caspase-dependent apoptosis inducer STS displayed similar cell death levels (Fig. 6B, right histogram), confirming that the single genetic ablation of Bax or Bak does not confer resistance to apoptotic PCD. Therefore, it seems that, in contrast to classical apoptosis, specific ablation of Bax in programmed necrosis is sufficient

(C) WT and *Capn4*$^{-/-}$ MEFs were not treated (Co) or treated with MNNG (12 h), and the levels of cell death were measured by PI staining. The data shown are the means ± SDs of the results ($n = 6$). (D) The levels of tAIF release were detected in cytosolic extracts purified from WT and *Capn4*$^{-/-}$ MEFs treated as described for panel C. Equal loading was verified by actin reblotting. (E) WT and *Capn4*$^{-/-}$ MEFs were treated as above, stained for the detection of 3′-OH DNA breaks, and analyzed by flow cytometry. The data shown are the means ± SDs of the results of three independent experiments. (F) Fluorescence assessment of calpain activity measured in WT and *Capn4*$^{-/-}$ MEFs not treated (Control) or treated with MNNG (1 h). Phase-contrast analysis was used to visualize cells. Representative micrographs of each treatment are shown. This experiment was repeated four times, yielding similar results. Bar, 10 μm. (G) Fluorometric analysis of calpain activity observed in cytosolic extracts obtained from WT and *Capn4*$^{-/-}$ MEFs treated with MNNG for the indicated times. The basal level of calpain activity observed in untreated WT cells is referred to as 1 unit. The data shown are the means ± SDs of the results ($n = 4$). (H) Immunoblotting assessment of levels of μ-calpain (μ-calp) in WT and *Capn4*$^{-/-}$ MEFs not treated or treated with MNNG (9 h). MNNG induced a significant decrease in the amount of the 80-kDa proform of μ-calpain in WT MEFs, but not in *Capn4*$^{-/-}$ MEFs.

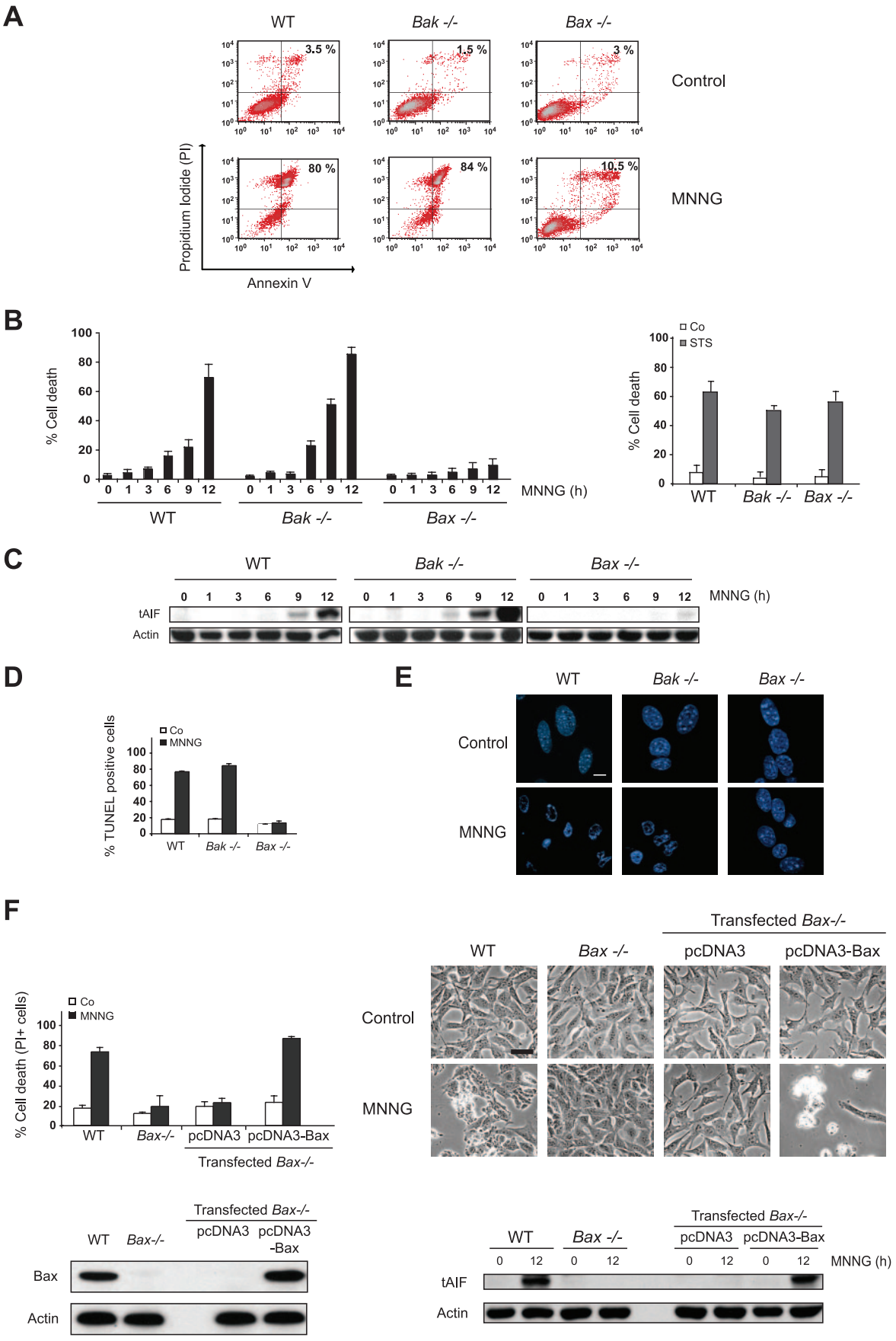
A
WT
Bak -/-
Bax -/-
3.5 %
1.5 %
3 %
Control
80 %
84 %
10.5 %
MNNG
Propidium Iodide (PI)
Annexin V
B
% Cell death
MNNG (h)
WT
Bak -/-
Bax -/-
Co
STS
C
tAIF
Actin
D
% TUNEL positive cells
Co
MNNG
E
Control
MNNG
F
% Cell death (PI+ cells)
Transfected Bax-/-
pcDNA3
pcDNA3-Bax
Bax
Actin

to preclude cell death. In MNNG-induced necrosis, Bax, but not Bak, deficiency disabled tAIF release from mitochondria to the cytosol (Fig. 6C). Consequently, MNNG-treated *Bax*$^{-/-}$ cells were TUNEL negative and did not present signs of nuclear chromatin condensation (Fig. 6D and E). Finally, to confirm that AIF release and necrosis were due to the specific lack of Bax, we reintroduced Bax into the *Bax*$^{-/-}$ cells by transient transfection. As depicted in Fig. 6F, Bax transfection resensitized *Bax*$^{-/-}$ cells to MNNG-induced AIF release and necrosis. Together, our results identify Bax as a key component of the alkylating DNA damage-induced necrotic pathway.

Molecular ordering of PARP-1, calpains, and Bax in MNNG-induced necrosis. Further, we sought to determine the molecular ordering of PARP-1, calpains, and Bax activation in MNNG-induced necrosis. We first assessed the relationship between PARP-1 and Bax. As shown in Fig. 7A, we detected the PAR polymers in *Bax*$^{-/-}$ cells, as well as in WT MEFs. Consequently, cellular NAD^+ depletion occurred similarly in both types of cells. This indicated that PARP-1 is activated independently of Bax during MNNG-induced necrosis. Taking these results together with our earlier results (Fig. 5), we have therefore demonstrated that PARP-1 is activated upstream of both calpains and Bax during MNNG-induced death.

The relative sequence of calpains and Bax activation was next assessed by measuring calpain activity in MNNG-treated WT and *Bax*$^{-/-}$ cells and by assessing the levels of Bax activation in MNNG-treated WT and *Capn4*$^{-/-}$ MEFs. As depicted in Fig. 7B, calpains were activated similarly in WT and *Bax*$^{-/-}$ MEFs, meaning that Bax is dispensable for the calpain activation process. In contrast, we showed a time-dependent increase of activated Bax in WT, but not in *Capn4*$^{-/-}$, MNNG-treated cells (Fig. 7C). This was further substantiated by the use of immunoprecipitation and immunofluorescence approaches, which detected activated Bax in MNNG-treated WT but not *Capn4*$^{-/-}$ cells (Fig. 7D and E). The results obtained by using these three independent methods indicated that Bax activation depends on calpains. Bax is thus activated downstream of calpains in MNNG-induced cell death.

MNNG induces Bax translocation from cytosol to mitochondria. To investigate the impact of Bax activation in MNNG-induced necrosis, we analyzed its subcellular redistribution. Immunofluorescence detection revealed a diffuse pattern of Bax distribution in untreated cells, which is compatible with the cytosolic localization of the soluble inactive protein (20, 76, 80) (Fig. 8A). Upon the induction of necrosis with MNNG, the diffuse pattern of fluorescence is replaced by a granular/punctate pattern that colocalizes with mitochondrial protein Cox IV (Fig. 8A), indicating that Bax relocalizes from the cytosol to mitochondria after MNNG treatment. This interpretation was fully confirmed by subcellular fractionation. Mitochondria and cytosol from WT MEFs induced to undergo cell death in response to MNNG or STS were purified. As shown in Fig. 8B, Bax is localized in the cytosol of untreated cells. However, upon stimulation with MNNG or STS, a significant fraction of Bax redistributes to mitochondria. Indeed, the Bax redeployment correlated strictly with the above-described Bax activation (Fig. 7) and the necrotic response of MEFs to MNNG treatment (Fig. 1 and 8A). In this sense, Bax mitochondrial redistribution was not observed in *PARP-1*$^{-/-}$ and *Capn4*$^{-/-}$ MNNG-resistant cells (Fig. 8A, right panels).

Overall, our data demonstrate that MNNG treatment induces a PARP-1/calpain-dependent conformational change of Bax, which provokes its activation and translocation to mitochondria. The presence of Bax in mitochondria results in mitochondrial perturbation, as evidenced by the loss of $\Delta\Psi_m$.

Bcl-2 regulates MNNG-induced necrosis. The importance of the Bcl-2 family of proteins in the control of alkylating DNA damage-mediated necrosis was further assessed in cells overexpressing Bcl-2. Indeed, it has been reported that Bcl-2 prevents Bax-dependent PCD by blocking dimerization of the protein in mitochondria (3, 14, 26, 38, 41, 43, 73, 76). Moreover, Bcl-2 controls mitochondrial AIF release in apoptotic conditions (50, 69–71) and Bcl-2 is also able to inhibit certain forms of necrotic cell death (34, 65–67), suggesting that apoptosis and necrosis share common Bax/Bcl-2 steps. As shown in the kinetic analysis included in Fig. 8C, after MNNG treatment, the viability of Bcl-2-overexpressing cells was superior to that of WT (Neo-transfected) cells. Importantly, Bcl-2 overexpression disabled tAIF release from mitochondria to the cytosol after MNNG treatment (Fig. 8D). Consequently, MNNG-treated Bcl-2-overexpressing cells were TUNEL negative and did not present signs of nuclear chromatin condensation (data not shown). Finally, to confirm that the inhibiting effect of Bcl-2 in MNNG-induced necrosis was due to the

FIG. 6. Bax, but not Bak, is necessary for AIF release and MNNG-induced necrosis. (A) WT, *Bax*$^{-/-}$, and *Bak*$^{-/-}$ cells were not treated (Control) or treated with MNNG (12 h), labeled with annexin V-FITC and PI, and analyzed by flow cytometry. Representative cytofluorometric plots are shown. The percentages refer to the frequencies of double-positive staining. (B) Kinetic analysis of PS exposure and loss of cell viability induced by MNNG in WT, *Bax*$^{-/-}$, and *Bak*$^{-/-}$ MEFs (left panel). After the indicated times, the cells were stained as described for panel A, and the frequencies of annexin V and PI double-positive labeling were recorded and expressed as percentages. STS was used as an apoptosis inducer (right panel). The data shown are the means ± standard deviations (SDs) of the results of five independent experiments. (C) Cytosolic fractions from MNNG-treated WT, *Bax*$^{-/-}$, and *Bak*$^{-/-}$ cells were blotted for tAIF detection. The actin levels were analyzed for a loading control. (D) WT, *Bax*$^{-/-}$, and *Bak*$^{-/-}$ MEFs were not treated (Co) or treated with MNNG (12 h), stained for the detection of 3′-OH DNA breaks, and analyzed by flow cytometry. The data shown are the means ± SDs of four independent experiments. (E) WT, *Bax*$^{-/-}$, and *Bak*$^{-/-}$ MEFs were treated with MNNG (9 h) and stained with Hoechst 33342 to visualize the nuclei. Representative nuclei from untreated (Control) or MNNG-treated cells are shown. Bar, 10 μm. (F) *Bax*$^{-/-}$ MEFs were transiently transfected with the indicated expression plasmids (pcDNA3 or pcDNA3-Bax) in the presence of QVD (10 μM) to prevent caspase-dependent PCD. Twelve hours after the indicated transfections, the MEFs were not treated (Control) or treated with MNNG (12 h). The levels of cell death were determined by PI staining. The data shown are the means ± SDs of the results ($n = 4$) (upper left panel). Representative microphotographs from each treatment are shown (upper right panel). Bar, 40 μm. The expression levels of Bax before and after the indicated transfections were assessed by immunoblotting (lower left panel). Cytosolic fractions from untreated or MNNG-treated WT, *Bax*$^{-/-}$, *Bax*$^{-/-}$ transfected with pcDNA3, or pcDNA3-Bax were immunoblotted for tAIF detection (lower right panel). Equal loading was confirmed by actin assessment.

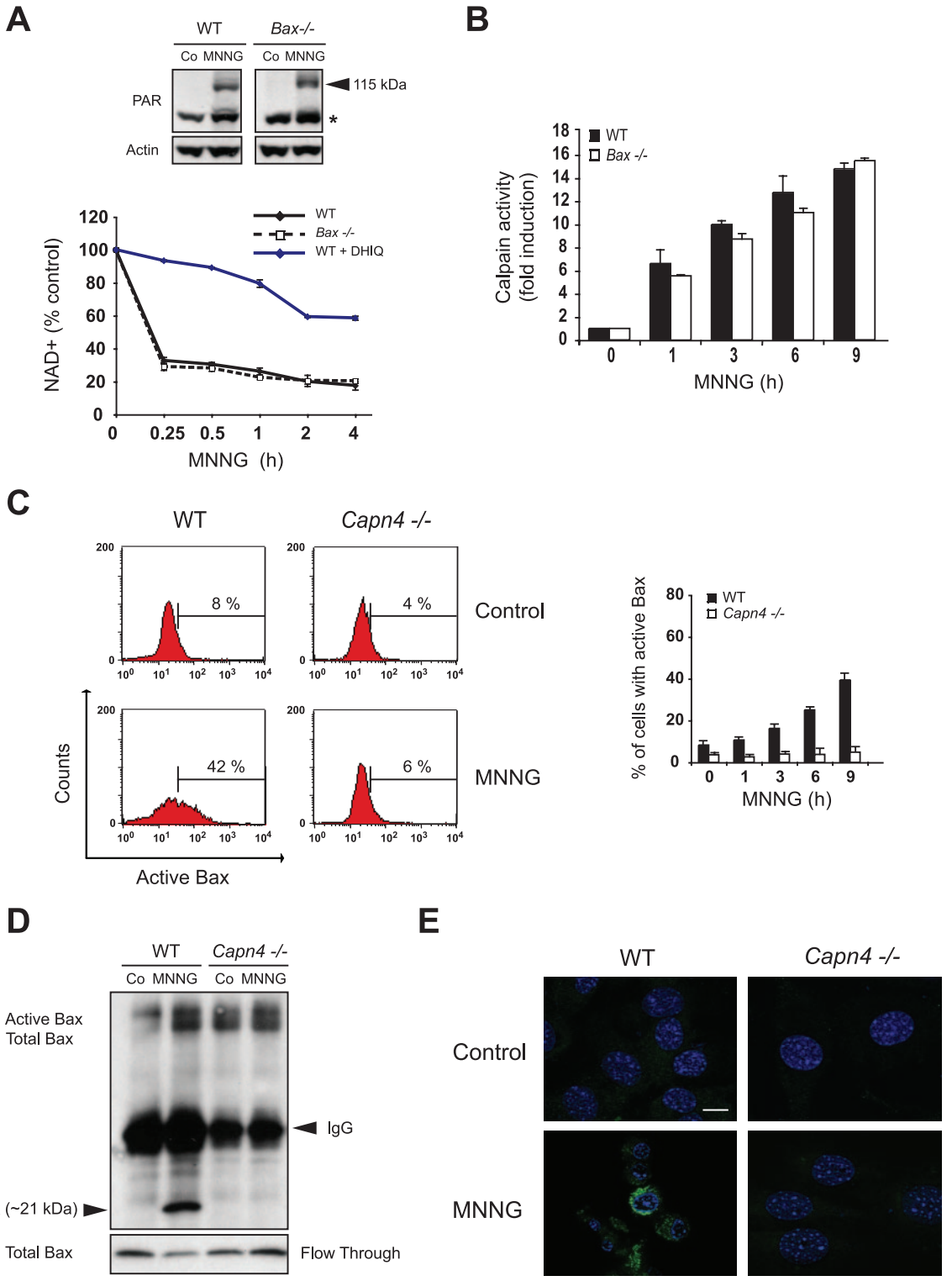

FIG. 7. Calpains are activated downstream of PARP-1 but upstream of Bax during MNNG-induced necrosis. (A) Detection of PAR by immunoblotting (115-kDa band) in total extracts from WT and *Bax*$^{-/-}$ MEFs not treated (Co) or treated with MNNG (15 min) (upper panel). The asterisk marks a nonspecific band. The membrane was reblotted for actin to control for protein loading. Alternatively, WT and *Bax*$^{-/-}$ MEFs were preincubated or not with DHIQ, treated with MNNG for the indicated times, and analyzed by measuring absorbance at 570 nm to assess total NAD^+ levels (lower panel). The concentrations of NAD^+ were normalized to those of untreated cells. The results shown are the means ± standard deviations (SDs) of the results of four independent experiments. (B) A fluorometric analysis of the levels of calpain activities was performed for extracts obtained from WT and *Bax*$^{-/-}$ MEFs treated with MNNG for the indicated times. The basal level of calpain activity observed in untreated cells is referred to as 1 unit. The results shown are the means ± SDs of the results of three independent experiments. (C) WT and *Capn4*$^{-/-}$ MEFs were treated with MNNG for the indicated times, and the levels of Bax activation were measured by flow cytometry (right panel). The data shown

specific action of the protein on mitochondria (e.g., abolishing tAIF mitochondrial release), we demonstrated that, even if PARP-1 and calpains remained activated (Fig. 8E), mitochondrial function (e.g., $\Delta\Psi_m$) was maintained in Bcl-2-overexpressing cells after MNNG treatment (Fig. 8C). Taking these results together with our above-described results, we revealed that Bcl-2 and Bax present opposing effects in regulating mitochondrial features characterizing MNNG-induced necrosis.

Collectively, the results presented here establish a novel molecular mechanism for alkylating DNA damage-induced cell death, a Bcl-2-controlled necrotic process. MMNG induces PARP-1 activity, which leads to calpain activation, which in turn regulates Bax activation and the conversion of AIF to tAIF. Active Bax is required for MOMP and AIF release. Upon transfer into the nucleus, tAIF causes 3′-OH DNA breaks and necrosis (Fig. 9).

DISCUSSION

Nitrosoureas are a developed group of alkylating DNA-damaging agents, which are best represented by MNNG. These agents are active anticancer drugs (61). It is well established that PARP-dependent translocation of the mitochondrial protein AIF to the nucleus is required in MNNG-induced necrosis. However, the molecular mechanism triggered by MNNG to induce AIF release and necrosis is unknown. In this report, we provide novel insights into this molecular mechanism, which includes the sequential activation of PARP-1, calpains, Bax, and AIF in a single cell death pathway. Our data, obtained in a large panel of MEF cells, demonstrate that MNNG-mediated necrosis proceeds via the induction of cellular alterations that are independent of some of the major apoptotic effectors, such as the caspases. Nevertheless, MNNG-induced necrotic PCD shares common features with the apoptotic form of cell death. Certain biochemical features are conserved, namely, outer leaflet exposure of PS in the plasma membrane or alterations to mitochondria (e.g., $\Delta\Psi$ loss or tAIF release). In addition, as for apoptosis, necrosis associated with alkylating DNA damage is dependent on the input from different cellular compartments. First, the nucleus, through PARP-1 activation; second, the cytosol, through calpain and Bax activities; and finally, mitochondria, through the Bcl-2-controlled tAIF release.

Traditionally, death associated with MNNG was attributable to the fact that PARP-1 activation correlated with a rapid cellular depletion of NAD^+ and ATP. Two major ATP generation mechanisms involving NAD^+ exist in a cell: (i) glycolysis, which uses cytosolic NAD^+ as a substrate, and (ii) mitochondrial oxidative phosphorylation, which uses mitochondrial NAD^+. Cytosolic and mitochondrial NAD^+ are not exchanged. In interleukin-3 (IL-3)-dependent hematopoietic cells, IL-3 deprivation, glucose withdrawal, or glycolytic blockade renders MNNG inefficient (88). Moreover, IL-3 deprivation, which blocks cellular glycolysis and the generation of the NAD^+ cytosolic pool, preserves ATP levels after MNNG treatment. This suggests that the glycolytic control of the metabolic state of the cell regulates DNA damage-mediated death (46, 88, 89). Our results with MEFs fully confirm these data. We first demonstrated that glucose deprivation or oxidative phosphorylation inhibition does not preclude cellular ATP generation. MEFs use glycolysis or mitochondrial oxidative phosphorylation to support their energetic needs. However, only MEFs using glycolysis are sensitized for alkylating DNA damage-induced necrosis; cells using oxidative phosphorylation (e.g., MEFs cultured in the absence of glucose) are significantly protected from MNNG treatment. Therefore, it seems that PARP-1 uses the glycolytic/cytosolic pool of NAD^+ to control MNNG-induced necrosis.

New studies confirm the hypothesis that energy collapse is not the sole mechanism by which PARP contributes to cell death. A "death link" between PARP, mitochondria, and AIF has been clearly established (16). More recently, a report established that PAR polymers produced by PARP-1 play an essential role in AIF-mediated necrosis (84). Our current results confirm the p53-independent role of PARP-1 (and not PARP-2) in the release of tAIF from mitochondria. Thus, it seems that the level (or the nature) of PAR polymers produced by PARP-1 is essential in MNNG-induced cell death. Polymers synthesized by the other members of the PARP family, such as PARP-2, were unable to activate the AIF-mediated necrotic pathway. Our data strongly favor the hypothesis that the complexity and concentration of each structural type of PAR may vary depending on the PARP implicated (31). Given the complexity of PAR structures and the existence of distinct PARP enzymes, this heterogeneity seems to reflect the different signaling functions of PARP family members and the specificities of PAR signaling pathways. Most importantly, we demonstrate that tAIF release depends on PARP-1-mediated calpain and Bax activation. Further analysis is therefore necessary to unravel the nature of the PAR polymers produced by PARP-1 and the relationships between these polymers and calpain and Bax activation. In any case, the specificity of the PARP-1 activation and the control of the AIF mitochondrial redistribution mediated by the calpain cysteine proteases and the proapoptotic member of the Bcl-2 family of proteins, Bax, are essential to an understanding of the interplay between the multiple MNNG-induced signals. The old concept of PARP-1 as a passive killer instigated by DNA damage could be replaced by its emerging role as an active key participant in a novel, molecularly orchestrated form of PCD.

are the means ± SDs of the results ($n = 5$). Representative cytofluorometric plots of the results for untreated (Control) and MNNG-treated (9 h) cells are shown (left panel). (D) WT and *Capn4*$^{-/-}$ MEFs were not treated (Co) or treated with MNNG (12 h), and then Bax was immunoprecipitated from the cell lysates by using an antibody specific for the active form of Bax. Samples were then analyzed by Bax immunoblotting. The unbound fraction for each condition was also blotted for Bax detection. The results illustrated are representative of three independent experiments. The molecular mass of Bax is shown on the left. (E) Immunofluorescence staining of activated Bax detected in WT and *Capn4*$^{-/-}$ MEFs not treated (Control) or treated with MNNG (9 h). A representative overlay of activated Bax and Hoechst 33342 nuclear staining is shown. Note that activated Bax was detected in MNNG-treated WT but not in *Capn4*$^{-/-}$cells. This experiment was repeated five times, yielding similar results. Bar, 10 μm.

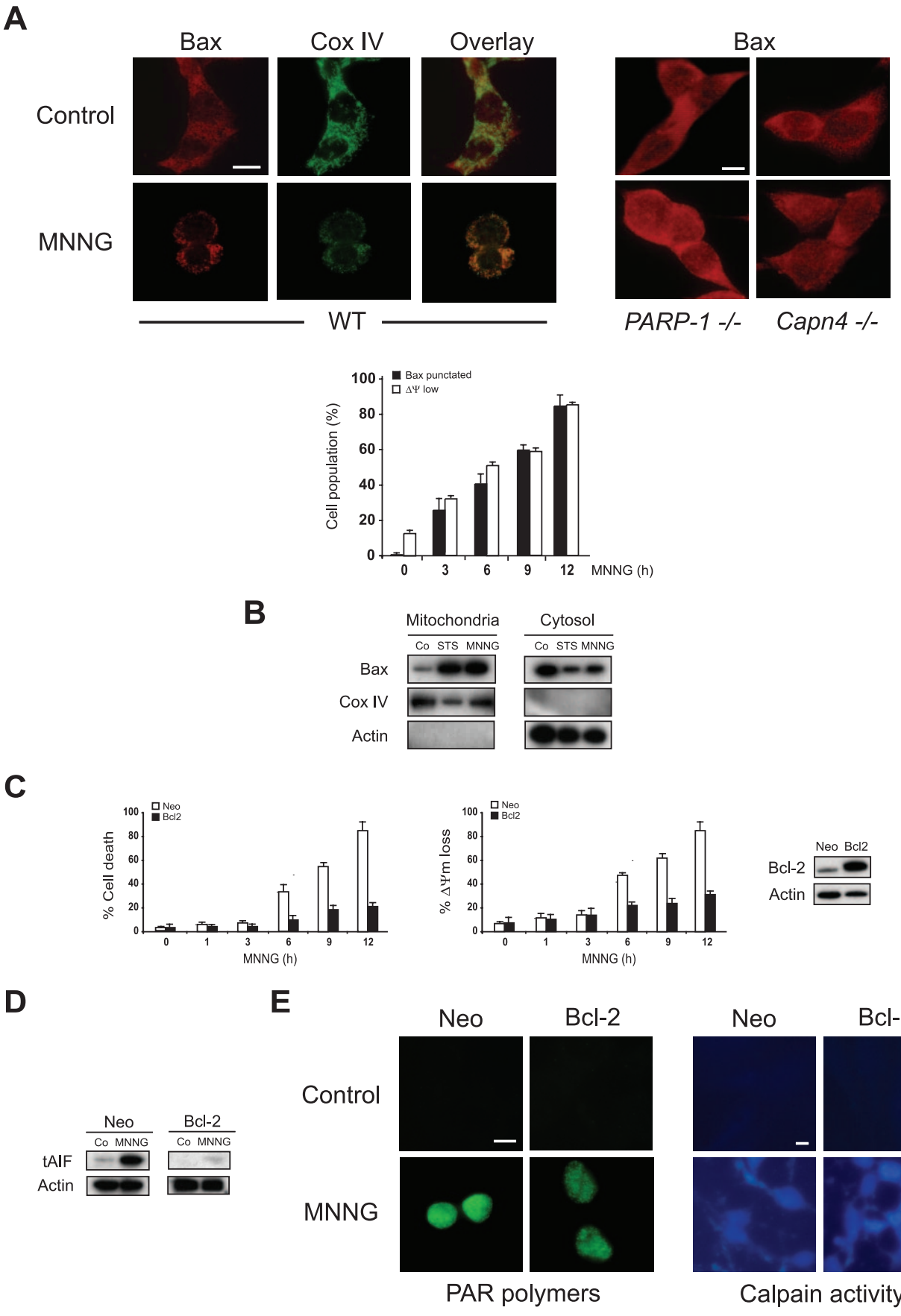
A
Bax
Cox IV
Overlay
Bax
Control
MNNG
WT
PARP-1 -/-
Capn4 -/-
Bax punctated
ΔΨ low
Cell population (%)
MNNG (h)
B
Mitochondria
Cytosol
Co STS MNNG
Co STS MNNG
Bax
Cox IV
Actin
C
Neo
Bcl2
% Cell death
MNNG (h)
% ΔΨm loss
MNNG (h)
Neo Bcl2
Bcl-2
Actin
D
Neo
Bcl-2
Co MNNG
Co MNNG
tAIF
Actin
E
Neo
Bcl-2
Neo
Bcl-2
Control
MNNG
PAR polymers
Calpain activity

Bcl-2 proteins are the main regulators of the mitochondrial death pathway. They can either suppress or promote mitochondrial changes by regulating the release of key proteins from mitochondria. Thus, the Bcl-2 family determines the cellular susceptibility to PCD (14). How Bcl-2 family proteins control the release of mitochondrial proteins is still unclear. However, it is clear that multidomain proapoptotic proteins such as Bax and Bak participate in this release (37, 41). Bax activation or Bak conformational changes lead to the formation of a mitochondrial pore that facilitates the release of mitochondrial proapoptotic proteins. Therefore, in apoptotic PCD, the combined genetic ablation of both Bax and Bak confer resistance to apoptosis (79). Strikingly, we find that, in alkylating DNA damage-induced necrosis, the single genetic inactivation of Bax precludes AIF release and necrosis. Thus, in this form of PCD, Bax is necessary, but Bak is dispensable. Despite the structural similarities and the genetically demonstrated redundancy in apoptosis of Bax and Bak (62), these data support the hypothesis that Bax and Bak do not perform redundant functions in all cell death models (5, 19). We also prove that, like apoptosis, necrosis could be a Bcl-2-controlled process. The mechanisms by which Bcl-2 inhibits apoptosis are only partially elucidated. Most experimental data suggest that Bcl-2 has to act on mitochondrial membranes to prevent apoptosis (14, 22, 25, 26, 38, 41, 64, 73, 76). On the one hand, Bcl-2 prevents the apoptosis-associated release of proapoptotic proteins from the mitochondrial intermembrane space via the outer mitochondrial membrane. In addition to this effect on the outer mitochondrial membrane, Bcl-2 prevents the disruption of the inner $\Delta\Psi_m$ during apoptosis. Our data reveal that, in programmed necrosis, Bcl-2 prevents cell death in a similar way: (i) by maintaining the subcellular compartmentalization of AIF and (ii) by stabilizing the $\Delta\Psi_m$. These findings demonstrate a previously unknown role of Bcl-2 in the regulation of necrotic PCD, in addition to the well-known role of this protein in apoptotic PCD.

In light of our results, calpain appears to link PARP-1 activity to Bax activation and AIF release during MNNG-induced necrosis. Recently, Bax has been identified as a target of calpains, suggesting that the generation of the 18-kDa Bax fragment by calpains is an early event in the induction of apoptosis via calpains, Bax, and mitochondria (2, 24, 81). However, p21 Bax is not cleaved into p18 Bax in MNNG-mediated PCD (R. S. Moubarak, V. J. Yuste, and S. A. Susin, unpublished observation). Thus, calpains control Bax activation via a yet-unknown mechanism in alkylating DNA damage-mediated necrosis. Concerning the cleavage of AIF into tAIF, three previous reports have shown that AIF is a membrane-integrated mitochondrial protein that becomes a soluble and proapoptotic protein after its cleavage by calpain and/or cathepsins (50, 54, 86). Remarkably, the present results indicate that calpain, and not cathepsins, controls mitochondrial AIF release during MNNG-induced death. As PARP-1-dependent MNNG-induced death does not promote lysosomal membrane permeabilization, cathepsins would therefore be excluded from this cell death pathway.

Little is known about the upstream mechanisms which regulate tAIF release from mitochondria. Our data suggest that this process requires the cooperative upstream action of calpains and Bax. On the one hand, calpains cleave AIF, yielding tAIF. On the other hand, Bax facilitates the MOMP that is necessary for AIF release. Consequently, even if calpains were activated in *Bax*$^{-/-}$ cells (Fig. 7), AIF would not be released from mitochondria to the cytosol. Thus, in characterizing calpains and Bax as the main elements in alkylating DNA damage-induced necrosis, we also provide the first insights into the molecular pathway governing tAIF release from mitochondria.

During apoptotic PCD, a number of distinct DNA condensation and fragmentation events take place. Two different degrees of chromatin condensation have been defined, partial chromatin condensation (stage I) and condensation into pyknotic apoptotic bodies (stage II) (60, 68). In necrotic PCD, our results demonstrated that MNNG-treated MEFs displayed stage I of chromatin condensation. The level of this nuclear modification correlated with the level of TUNEL-positive DNA fragmentation. Importantly, we showed that these two nuclear alterations were caused by AIF. Indeed, by knockdown of AIF, we demonstrated that the action of nuclear-translo-

FIG. 8. The Bcl-2 family of proteins regulates MNNG-mediated necrosis through opposing effects of Bax and Bcl-2 on mitochondria. (A) WT MEFs were left untreated (Control) or treated with MNNG for 6 h and stained for the detection of Bax and Cox IV (used as a mitochondrial marker) before being examined by fluorescence microscopy (left panel). These representative cells show that Bax has a cytosolic distribution in control cells, whereas it colocalizes with Cox IV in MNNG-treated cells. The experiment was repeated three times with low variability in the results (<5%). Bar, 10 μm. In contrast to WT cells, in *PARP-1*$^{-/-}$ and *Capn4*$^{-/-}$ MEFs, Bax remains cytosolic after MNNG treatment (right panel). Alternatively, the number of cells presenting low $\Delta\Psi_m$ (measured by flow cytometry) or punctated Bax were quantified and plotted as percentages of total cells (graph). The data shown are the means ± SDs of the results of five independent experiments. Bar, 10 μm. (B) Mitochondrial and cytosolic extracts of cells not treated (Co) or treated with MNNG (6 h) were analyzed by Western blotting for the presence of Bax. Cox IV and actin were used as controls for fractionation quality and protein loading. This experiment was repeated four times, yielding comparable results. STS was used as a positive control. (C) Cells stably transfected with vector only (Neo) or the cDNA coding for Bcl-2 were left untreated or treated with MNNG at the indicated times and stained with annexin V-FITC and PI, and the frequencies of double-positive labeling were recorded and pictured as a plot. The data shown are the means ± SDs of the results of five independent experiments (left panel). In a similar experiment, WT or Bcl-2-overexpressing cells were treated with MNNG for the indicated times and then labeled with TMRE and assessed for the loss of $\Delta\Psi_m$. The results shown are the means ± SDs of the results of three independent experiments (middle panel). Bcl-2 overexpression was confirmed by immunoblotting (right panel). (D) tAIF detection in cytosolic extracts purified from WT and Bcl-2-overexpressing cells treated as described for panel C. Note that tAIF was detected in MNNG-treated WT cells but not in Bcl-2-overexpressing cells. Actin detection was used as a loading control. (E) WT and Bcl-2-overexpressing cells were not treated (Control) or treated with MNNG (15 min), immunostained for PAR detection (green) as described for Fig. 3, and examined by fluorescence microscopy (left panel). Representative micrographs of each cell type are shown. This experiment was repeated three times, yielding similar results. Bar, 10 μm. A fluorescence assessment of calpain activity measured in WT and Bcl-2-overexpressing cells not treated (Control) or treated with MNNG (1 h) as described for Fig. 4 was performed (right panel). Micrographs of representative cells after each treatment are shown. This experiment was repeated three times, yielding comparable results. Bar, 10 μm.

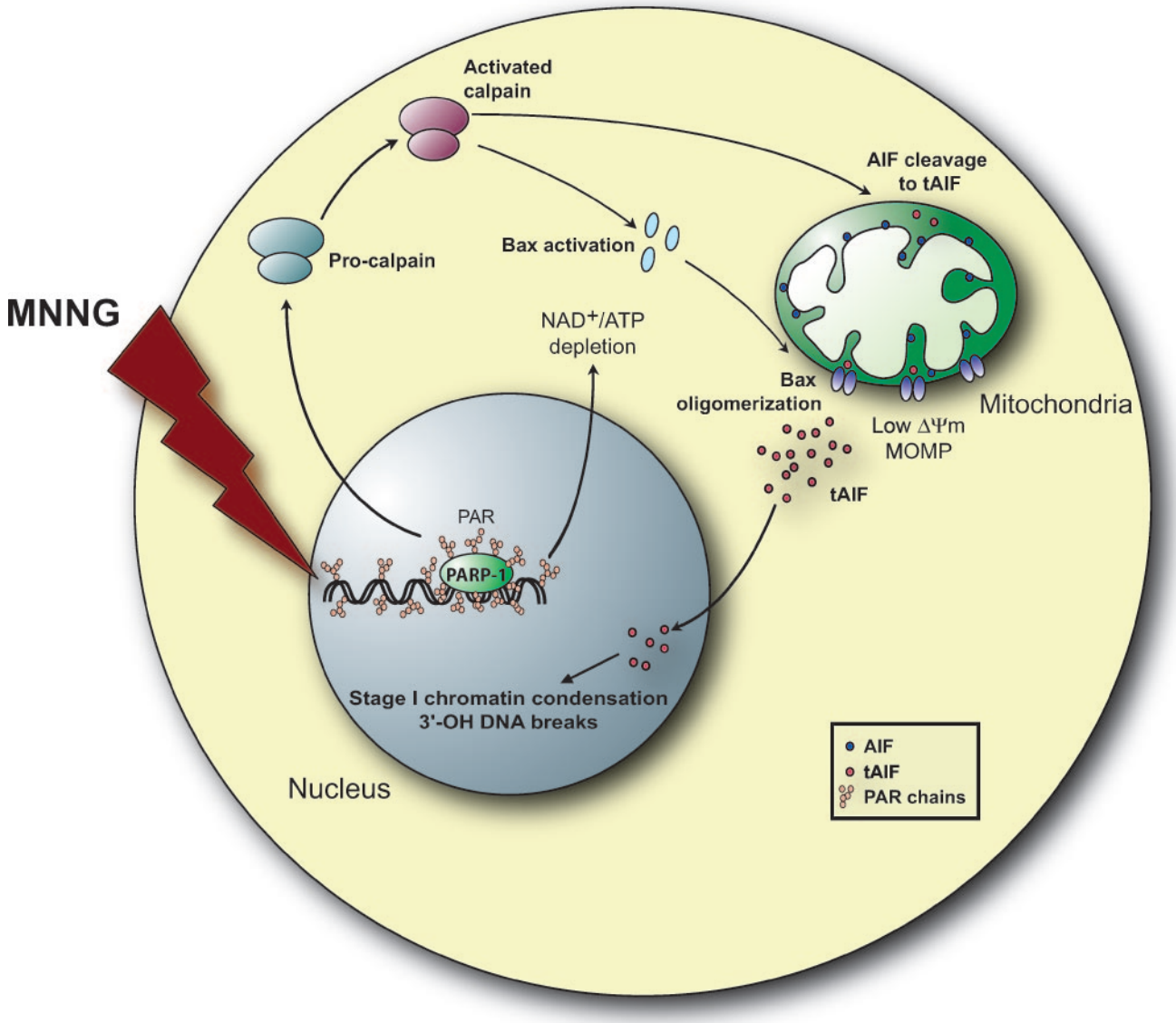

FIG. 9. Schematic model for MNNG-induced cell death. MNNG-induced DNA damage leads through PARP-1 to calpain activation. Calpain in turn activates Bax, resulting in its translocation from the cytosol to mitochondria, where it facilitates the release of tAIF from the mitochondrial intermembrane space to the cytosol. The activated calpain also regulates AIF release by cleaving the membrane-anchored AIF to the soluble form tAIF. Once liberated in the cytosol, tAIF translocates to the nucleus, where it generates 3′-OH DNA breaks and stage I of chromatin condensation.

cated AIF was crucial in alkylating DNA damage-induced necrosis. This is an important issue that sheds new light on the role of AIF in PCD.

Controversies still exist regarding which model of PCD is important in cell regulation. Partial resolution of these controversies may come with the recognition that apoptosis and necrosis frequently represent alternate outcomes of a similar pathway, particularly for cell death mediated by Bcl-2 proteins (e.g., Bax/Bcl-2) or proapoptotic mitochondrial proteins (e.g., AIF). This report confirms that, similar to apoptosis, necrosis could be a regulated form of PCD. This necrotic program can occur in cells possessing an intact mechanism of apoptotic cell destruction (e.g., STS-mediated apoptosis). This implies the existence of a necrotic signaling pathway that could be modulated independently from the classical apoptotic pathway. Of note, many tumors carry alterations inactivating the apoptosis pathway (e.g., p53 mutations). Based on our current results, it seems conceivable that this alternative necrotic pathway might be activated to induce cell death in these tumor cells (e.g., by using Bax-derived peptides to provoke AIF mitochondrial release). In this sense, our results might pave the way for the development of novel pharmacological tools to circumvent the commonly observed chemotherapy resistance of transformed cells. In addition, DNA damage-induced necrosis occurs selectively in growing cells, not in vegetative cells (88, 89). Indeed, cells grown to confluence were less sensitive to alkylating DNA damage-mediated death than subconfluent cells. Because uncontrolled and invasive growth defines a key characteristic of

tumor cells, our results on DNA damage-mediated necrosis could provide an important consideration for exploiting this type of PCD in cancer control. In this context, it is important to underline that only cells using aerobic glycolysis, which is also typical in cancer cells (89), are sensitized to MNNG-induced death. Thus, our study on PARP-1, calpains, Bax, and AIF provides a new angle of analysis for the development of novel tumor cell-specific therapeutic agents.

Overall, this report provides substantial progress in the understanding of (i) the molecular events regulating alkylating DNA damage-induced cell death, (ii) the molecular mechanisms which control mitochondrial release of AIF, and (iii) a novel signaling pathway which distinguishes necrosis from apoptotic PCD.

ACKNOWLEDGMENTS

We thank V. L. Dawson, S. J. Korsmeyer, A. Rudensky, and Y. Tan for cells, S. Matsuyama for the pcDNA3-Bax plasmid, J. L. Fernandez-Luna for the Bcl-2 insert, S. Barbier, S. Beaucourt, M. Bras, F. J. del Castillo, N. Robert, P. Sancho, and C. Solé for helpful assistance, and M. Cohen-Salmon, G. de Murcia, G. Eberl, and M. Segade for critical reading of the manuscript.

This work was supported by institutional grants from Institut Pasteur and CNRS and by specific grants from Fondation de France Ligue Contre le Cancer, and Association pour la Recherche sur le Cancer (ARC: contract 4043) (to S.A.S.). R.S.M. received Ph.D. fellowships from Fondation Hariri and ARC. V.J.Y. was supported by a Marie Curie fellowship (contract MEIF-2003-501887).

We declare that we have no competing financial interests.

REFERENCES

1. **Alano, C. C., W. Ying, and R. A. Swanson.** 2004. Poly(ADP-ribose) polymerase-1-mediated cell death in astrocytes requires NAD^+ depletion and mitochondrial permeability transition. J. Biol. Chem. **279:**18895–18902.
2. **Altznauer, F., S. Conus, A. Cavalli, G. Folkers, and H. U. Simon.** 2004. Calpain-1 regulates Bax and subsequent Smac-dependent caspase-3 activation in neutrophil apoptosis. J. Biol. Chem. **279:**5947–5957.
3. **Antonsson, B., S. Montessuit, S. Lauper, R. Eskes, and J. C. Martinou.** 2000. Bax oligomerization is required for channel-forming activity in liposomes and to trigger cytochrome *c* release from mitochondria. Biochem. J. **345:** 271–278.
4. **Barkla, D. H., and P. R. Gibson.** 1999. The fate of epithelial cells in the human large intestine. Pathology **31:**230–238.
5. **Cartron, P. F., P. Juin, L. Oliver, S. Martin, K. Meflah, and F. M. Vallette.** 2003. Nonredundant role of Bax and Bak in Bid-mediated apoptosis. Mol. Cell. Biol. **23:**4701–4712.
6. **Chan, F. K., J. Shisler, J. G. Bixby, M. Felices, L. Zheng, M. Appel, J. Orenstein, B. Moss, and M. J. Lenardo.** 2003. A role for tumor necrosis factor receptor-2 and receptor-interacting protein in programmed necrosis and antiviral responses. J. Biol. Chem. **278:**51613–51621.
7. **Chautan, M., G. Chazal, F. Cecconi, P. Gruss, and P. Golstein.** 1999. Interdigital cell death can occur through a necrotic and caspase-independent pathway. Curr. Biol. **9:**967–970.
8. **Cheung, E. C., N. Joza, N. A. Steenaart, K. A. McClellan, M. Neuspiel, S. McNamara, J. G. Maclaurin, P. Rippstein, D. S. Park, G. C. Shore, H. M. McBride, J. M. Penninger, and R. S. Slack.** 2006. Dissociating the dual roles of apoptosis-inducing factor in maintaining mitochondrial structure and apoptosis. EMBO J. **25:**4061–4073.
9. **Colbourne, F., G. R. Sutherland, and R. N. Auer.** 1999. Electron microscopic evidence against apoptosis as the mechanism of neuronal death in global ischemia. J. Neurosci. **19:**4200–4210.
10. **Conde, C., M. Mark, F. J. Oliver, A. Huber, G. de Murcia, and J. Menissier-de Murcia.** 2001. Loss of poly(ADP-ribose) polymerase-1 causes increased tumour latency in p53-deficient mice. EMBO J. **20:**3535–3543.
11. **Corbiere, C., B. Liagre, F. Terro, and J. L. Beneytout.** 2004. Induction of antiproliferative effect by diosgenin through activation of p53, release of apoptosis-inducing factor (AIF) and modulation of caspase-3 activity in different human cancer cells. Cell Res. **14:**188–196.
12. **Cregan, S. P., V. L. Dawson, and R. S. Slack.** 2004. Role of AIF in caspase-dependent and caspase-independent cell death. Oncogene **23:**2785–2796.
13. **Cregan, S. P., A. Fortin, J. G. MacLaurin, S. M. Callaghan, F. Cecconi, S. W. Yu, T. M. Dawson, V. L. Dawson, D. S. Park, G. Kroemer, and R. S. Slack.** 2002. Apoptosis-inducing factor is involved in the regulation of caspase-independent neuronal cell death. J. Cell Biol. **158:**507–517.
14. **Danial, N. N., and S. J. Korsmeyer.** 2004. Cell death: critical control points. Cell **116:**205–219.
15. **Dantzer, F., J. C. Ame, V. Schreiber, J. Nakamura, J. Menissier-de Murcia, and G. de Murcia.** 2006. Poly(ADP-ribose) polymerase-1 activation during DNA damage and repair. Methods Enzymol. **409:**493–510.
16. **Dawson, V. L., and T. M. Dawson.** 2004. Deadly conversations: nuclear-mitochondrial cross-talk. J. Bioenerg. Biomembr. **36:**287–294.
17. **Delettre, C., V. J. Yuste, R. S. Moubarak, M. Bras, J. C. Lesbordes-Brion, S. Petres, J. Bellalou, and S. A. Susin.** 2006. AIFsh, a novel apoptosis-inducing factor (AIF) pro-apoptotic isoform with potential pathological relevance in human cancer. J. Biol. Chem. **281:**6413–6427.
18. **Delettre, C., V. J. Yuste, R. S. Moubarak, M. Bras, N. Robert, and S. A. Susin.** 2006. Identification and characterization of AIFsh2, a mitochondrial apoptosis-inducing factor (AIF) isoform with NADH oxidase activity. J. Biol. Chem. **281:**18507–18518.
19. **Deng, Y., Y. Lin, and X. Wu.** 2002. TRAIL-induced apoptosis requires Bax-dependent mitochondrial release of Smac/DIABLO. Genes Dev. **16:** 33–45.
20. **Dewson, G., R. T. Snowden, J. B. Almond, M. J. Dyer, and G. M. Cohen.** 2003. Conformational change and mitochondrial translocation of Bax accompany proteasome inhibitor-induced apoptosis of chronic lymphocytic leukemic cells. Oncogene **22:**2643–2654.
21. **Edinger, A. L., and C. B. Thompson.** 2004. Death by design: apoptosis, necrosis and autophagy. Curr. Opin. Cell Biol. **16:**663–669.
22. **Er, E., L. Oliver, P. F. Cartron, P. Juin, S. Manon, and F. M. Vallette.** 2006. Mitochondria as the target of the pro-apoptotic protein Bax. Biochim. Biophys. Acta **1757:**1301–1311.
23. **Feraud, O., N. Debili, J. M. Penninger, and G. Kroemer.** 2007. Cavitation of embryoid bodies requires optimal oxidative phosphorylation and AIF. Cell Death Differ. **14:**385–387.
24. **Gao, G., and Q. P. Dou.** 2000. N-terminal cleavage of Bax by calpain generates a potent proapoptotic 18-kDa fragment that promotes Bcl-2-independent cytochrome C release and apoptotic cell death. J. Cell. Biochem. **80:** 53–72.
25. **Green, D. R., and J. C. Reed.** 1998. Mitochondria and apoptosis. Science **281:**1309–1312.
26. **Gross, A., J. M. McDonnell, and S. J. Korsmeyer.** 1999. BCL-2 family members and mitochondria in apoptosis. Genes Dev. **13:**1899–1911.
27. **Guicciardi, M. E., S. F. Bronk, N. W. Werneburg, X. M. Yin, and G. J. Gores.** 2005. Bid is upstream of lysosome-mediated caspase 2 activation in tumor necrosis factor alpha-induced hepatocyte apoptosis. Gastroenterology **129:** 269–284.
28. **Haince, J. F., M. Rouleau, M. J. Hendzel, J. Y. Masson, and G. G. Poirier.** 2005. Targeting poly(ADP-ribosyl)ation: a promising approach in cancer therapy. Trends Mol. Med. **11:**456–463.
29. **Hart, L. S., D. Ornelles, and C. Koumenis.** 2007. The adenoviral e4orf6 protein induces atypical apoptosis in response to DNA damage. J. Biol. Chem. **282:**6061–6067.
30. **Harwood, S. M., M. M. Yaqoob, and D. A. Allen.** 2005. Caspase and calpain function in cell death: bridging the gap between apoptosis and necrosis. Ann. Clin. Biochem. **42:**415–431.
31. **Hassa, P. O., S. S. Haenni, M. Elser, and M. O. Hottiger.** 2006. Nuclear ADP-ribosylation reactions in mammalian cells: where are we today and where are we going? Microbiol. Mol. Biol Rev. **70:**789–829.
32. **Hengartner, M. O.** 2000. The biochemistry of apoptosis. Nature **407:**770–776.
33. **Holler, N., R. Zaru, O. Micheau, M. Thome, A. Attinger, S. Valitutti, J. L. Bodmer, P. Schneider, B. Seed, and J. Tschopp.** 2000. Fas triggers an alternative, caspase-8-independent cell death pathway using the kinase RIP as effector molecule. Nat. Immunol. **1:**489–495.
34. **Kane, D. J., T. Ord, R. Anton, and D. E. Bredesen.** 1995. Expression of bcl-2 inhibits necrotic neural cell death. J. Neurosci. Res. **40:**269–275.
35. **Kang, Y. H., M. J. Yi, M. J. Kim, M. T. Park, S. Bae, C. M. Kang, C. K. Cho, I. C. Park, M. J. Park, C. H. Rhee, S. I. Hong, H. Y. Chung, Y. S. Lee, and S. J. Lee.** 2004. Caspase-independent cell death by arsenic trioxide in human cervical cancer cells: reactive oxygen species-mediated poly(ADP-ribose) polymerase-1 activation signals apoptosis-inducing factor release from mitochondria. Cancer Res. **64:**8960–8967.
36. **Kim, W. J., D. I. Beardsley, A. W. Adamson, and K. D. Brown.** 2005. The monofunctional alkylating agent *N*-methyl-*N*′-nitro-*N*-nitrosoguanidine triggers apoptosis through p53-dependent and -independent pathways. Toxicol. Appl. Pharmacol. **202:**84–98.
37. **Kuwana, T., L. Bouchier-Hayes, J. E. Chipuk, C. Bonzon, B. A. Sullivan, D. R. Green, and D. D. Newmeyer.** 2005. BH3 domains of BH3-only proteins differentially regulate Bax-mediated mitochondrial membrane permeabilization both directly and indirectly. Mol. Cell **17:**525–535.
38. **Kuwana, T., and D. D. Newmeyer.** 2003. Bcl-2-family proteins and the role of mitochondria in apoptosis. Curr. Opin. Cell Biol. **15:**691–699.
39. **Liu, T., B. Brouha, and D. Grossman.** 2004. Rapid induction of mitochondrial events and caspase-independent apoptosis in Survivin-targeted melanoma cells. Oncogene **23:**39–48.

40. **Lorenzo, H. K., and S. A. Susin.** 2004. Mitochondrial effectors in caspase-independent cell death. FEBS Lett. **557:**14–20.
41. **Martinou, J. C., and D. R. Green.** 2001. Breaking mitochondrial barrier. Nat. Rev. Mol. Cell Biol. **2:**63–67.
42. **Menissier de Murcia, J., M. Ricoul, L. Tartier, C. Niedergang, A. Huber, F. Dantzer, V. Schreiber, J. C. Ame, A. Dierich, M. LeMeur, L. Sabatier, P. Chambon, and G. de Murcia.** 2003. Functional interaction between PARP-1 and PARP-2 in chromosome stability and embryonic development in mouse. EMBO J. **22:**2255–2263.
43. **Mikhailov, V., M. Mikhailova, D. J. Pulkrabek, Z. Dong, M. A. Venkatachalam, and P. Saikumar.** 2001. Bcl-2 prevents Bax oligomerization in mitochondrial outer membrane. J. Biol. Chem. **276:**18361–18374.
44. **Modjtahedi, N., F. Giordanetto, F. Madeo, and G. Kroemer.** 2006. Apoptosis-inducing factor: vital and lethal. Trends Cell Biol. **16:**264–272.
45. **Munoz-Pinedo, C., A. Guio-Carrion, J. C. Goldstein, P. Fitzgerald, D. D. Newmeyer, and D. R. Green.** 2006. Different mitochondrial intermembrane space proteins are released during apoptosis in a manner that is coordinately initiated but can vary in duration. Proc. Natl. Acad. Sci. USA **103:**11573–11578.
46. **Nelson, D. A., and E. White.** 2004. Exploiting different ways to die. Genes Dev. **18:**1223–1226.
47. **Nicotera, P., M. Leist, and L. Manzo.** 1999. Neuronal cell death: a demise with different shapes. Trends Pharmacol. Sci. **20:**46–51.
48. **Nicotera, P., and S. A. Lipton.** 1999. Excitotoxins in neuronal apoptosis and necrosis. J. Cereb. Blood Flow Metab. **19:**583–591.
49. **Nomura, M., N. Nomura, E. W. Newcomb, Y. Lukyanov, C. Tamasdan, and D. Zagzag.** 2004. Geldanamycin induces mitotic catastrophe and subsequent apoptosis in human glioma cells. J. Cell Physiol. **201:**374–384.
50. **Otera, H., S. Ohsakaya, Z. Nagaura, N. Ishihara, and K. Mihara.** 2005. Export of mitochondrial AIF in response to proapoptotic stimuli depends on processing at the intermembrane space. EMBO J. **24:**1375–1386.
51. **Pardee, A. B., Y. Z. Li, and C. J. Li.** 2002. Cancer therapy with beta-lapachone. Curr. Cancer Drug Targets **2:**227–242.
52. **Park, Y. C., J. H. Jeong, K. J. Park, H. J. Choi, Y. M. Park, B. K. Jeong, Y. Higuchi, and Y. H. Yoo.** 2005. Sulindac activates nuclear translocation of AIF, DFF40 and endonuclease G but not induces oligonucleosomal DNA fragmentation in HT-29 cells. Life Sci. **77:**2059–2070.
53. **Perrin, B. J., and A. Huttenlocher.** 2002. Calpain. Int. J. Biochem. Cell Biol. **34:**722–725.
54. **Polster, B. M., G. Basanez, A. Etxebarria, J. M. Hardwick, and D. G. Nicholls.** 2005. Calpain I induces cleavage and release of apoptosis-inducing factor from isolated mitochondria. J. Biol. Chem. **280:**6447–6454.
55. **Porter, A. G., and A. G. Urbano.** 2006. Does apoptosis-inducing factor (AIF) have both life and death functions in cells? Bioessays **28:**834–843.
56. **Proskuryakov, S. Y., A. G. Konoplyannikov, and V. L. Gabai.** 2003. Necrosis: a specific form of programmed cell death? Exp. Cell Res. **283:**1–16.
57. **Reix, S., N. Mechawar, S. A. Susin, R. Quirion, and S. Krantic.** 2007. Expression of cortical and hippocampal apoptosis-inducing factor (AIF) in aging and Alzheimer's disease. Neurobiol. Aging **28:**351–356.
58. **Roue, G., N. Bitton, V. J. Yuste, T. Montange, M. Rubio, F. Dessauge, C. Delettre, H. Merle-Beral, M. Sarfati, and S. A. Susin.** 2003. Mitochondrial dysfunction in CD47-mediated caspase-independent cell death: ROS production in the absence of cytochrome *c* and AIF release. Biochimie **85:**741–746.
59. **Saelens, X., N. Festjens, E. Parthoens, I. Vanoverberghe, M. Kalai, F. van Kuppeveld, and P. Vandenabeele.** 2005. Protein synthesis persists during necrotic cell death. J. Cell Biol. **168:**545–551.
60. **Samejima, K., S. Tone, and W. C. Earnshaw.** 2001. CAD/DFF40 nuclease is dispensable for high molecular weight DNA cleavage and stage I chromatin condensation in apoptosis. J. Biol. Chem. **276:**45427–45432.
61. **Schabel, F. M., Jr.** 1976. Nitrosoureas: a review of experimental antitumor activity. Cancer Treat. Rep. **60:**665–698.
62. **Scorrano, L., and S. J. Korsmeyer.** 2003. Mechanisms of cytochrome *c* release by proapoptotic BCL-2 family members. Biochem. Biophys. Res. Commun. **304:**437–444.
63. **Shall, S., and G. de Murcia.** 2000. Poly(ADP-ribose) polymerase-1: what have we learned from the deficient mouse model? Mutat. Res. **460:**1–15.
64. **Sharpe, J. C., D. Arnoult, and R. J. Youle.** 2004. Control of mitochondrial permeability by Bcl-2 family members. Biochim. Biophys. Acta **1644:**107–113.
65. **Shimizu, S., Y. Eguchi, W. Kamiike, S. Waguri, Y. Uchiyama, H. Matsuda, and Y. Tsujimoto.** 1996. Bcl-2 blocks loss of mitochondrial membrane potential while ICE inhibitors act at a different step during inhibition of death induced by respiratory chain inhibitors. Oncogene **13:**21–29.
66. **Shimizu, S., Y. Eguchi, W. Kamiike, S. Waguri, Y. Uchiyama, H. Matsuda, and Y. Tsujimoto.** 1996. Retardation of chemical hypoxia-induced necrotic cell death by Bcl-2 and ICE inhibitors: possible involvement of common mediators in apoptotic and necrotic signal transductions. Oncogene **12:**2045–2050.
67. **Strasser, A., A. W. Harris, and S. Cory.** 1991. bcl-2 transgene inhibits T cell death and perturbs thymic self-censorship. Cell **67:**889–899.
68. **Susin, S. A., E. Daugas, L. Ravagnan, K. Samejima, N. Zamzami, M. Loeffler, P. Costantini, K. F. Ferri, T. Irinopoulou, M. C. Prevost, G. Brothers, T. W. Mak, J. Penninger, W. C. Earnshaw, and G. Kroemer.** 2000. Two distinct pathways leading to nuclear apoptosis. J. Exp. Med. **192:**571–580.
69. **Susin, S. A., H. K. Lorenzo, N. Zamzami, I. Marzo, B. E. Snow, G. M. Brothers, J. Mangion, E. Jacotot, P. Costantini, M. Loeffler, N. Larochette, D. R. Goodlett, R. Aebersold, D. P. Siderovski, J. M. Penninger, and G. Kroemer.** 1999. Molecular characterization of mitochondrial apoptosis-inducing factor. Nature **397:**441–446.
70. **Susin, S. A., N. Zamzami, M. Castedo, E. Daugas, H. G. Wang, S. Geley, F. Fassy, J. C. Reed, and G. Kroemer.** 1997. The central executioner of apoptosis: multiple connections between protease activation and mitochondria in Fas/APO-1/CD95- and ceramide-induced apoptosis. J. Exp. Med. **186:**25–37.
71. **Susin, S. A., N. Zamzami, M. Castedo, T. Hirsch, P. Marchetti, A. Macho, E. Daugas, M. Geuskens, and G. Kroemer.** 1996. Bcl-2 inhibits mitochondrial release of an apoptogenic protease. J. Exp. Med. **184:**1331–1341.
72. **Tan, Y., N. Dourdin, C. Wu, T. De Veyra, J. S. Elce, and P. A. Greer.** 2006. Ubiquitous calpains promote caspase-12 and JNK activation during endoplasmic reticulum stress-induced apoptosis. J. Biol. Chem. **281:**16016–16024.
73. **Tsujimoto, Y.** 2002. Bcl-2 family of proteins: life-or-death switch in mitochondria. Biosci. Rep. **22:**47–58.
74. **Vahsen, N., C. Cande, J. J. Briere, P. Benit, N. Joza, N. Larochette, P. G. Mastroberardino, M. O. Pequignot, N. Casares, V. Lazar, O. Feraud, N. Debili, S. Wissing, S. Engelhardt, F. Madeo, M. Piacentini, J. M. Penninger, H. Schagger, P. Rustin, and G. Kroemer.** 2004. AIF deficiency compromises oxidative phosphorylation. EMBO J. **23:**4679–4689.
75. **Vanden Berghe, T., G. van Loo, X. Saelens, M. Van Gurp, G. Brouckaert, M. Kalai, W. Declercq, and P. Vandenabeele.** 2004. Differential signaling to apoptotic and necrotic cell death by Fas-associated death domain protein FADD. J. Biol. Chem. **279:**7925–7933.
76. **Vander Heiden, M. G., and C. B. Thompson.** 1999. Bcl-2 proteins: regulators of apoptosis or of mitochondrial homeostasis? Nat. Cell Biol. **1:**E209–E216.
77. **Vega-Manriquez, X., Y. Lopez-Vidal, J. Moran, L. G. Adams, and J. A. Gutierrez-Pabello.** 2007. Apoptosis-inducing factor participation in bovine macrophage *Mycobacterium bovis*-induced caspase-independent cell death. Infect. Immun. **75:**1223–1228.
78. **Wang, H., S. W. Yu, D. W. Koh, J. Lew, C. Coombs, W. Bowers, H. J. Federoff, G. G. Poirier, T. M. Dawson, and V. L. Dawson.** 2004. Apoptosis-inducing factor substitutes for caspase executioners in NMDA-triggered excitotoxic neuronal death. J. Neurosci. **24:**10963–10973.
79. **Wei, M. C., W. X. Zong, E. H. Cheng, T. Lindsten, V. Panoutsakopoulou, A. J. Ross, K. A. Roth, G. R. MacGregor, C. B. Thompson, and S. J. Korsmeyer.** 2001. Proapoptotic BAX and BAK: a requisite gateway to mitochondrial dysfunction and death. Science **292:**727–730.
80. **Wolter, K. G., Y. T. Hsu, C. L. Smith, A. Nechushtan, X. G. Xi, and R. J. Youle.** 1997. Movement of Bax from the cytosol to mitochondria during apoptosis. J. Cell Biol. **139:**1281–1292.
81. **Wood, D. E., and E. W. Newcomb.** 2000. Cleavage of Bax enhances its cell death function. Exp. Cell Res. **256:**375–382.
82. **Wsierska-Gadek, J., M. Gueorguieva, and J. Wojciechowski.** 2003. MNNG induces dramatic DNA damage and non-apoptotic changes in cervical carcinoma HeLa cells. Ann. N. Y. Acad. Sci. **1010:**278–282.
83. **Xu, Y., S. Huang, Z. G. Liu, and J. Han.** 2006. Poly(ADP-ribose) polymerase-1 signaling to mitochondria in necrotic cell death requires RIP1/TRAF2-mediated JNK1 activation. J. Biol. Chem. **281:**8788–8795.
84. **Yu, S. W., S. A. Andrabi, H. Wang, N. S. Kim, G. G. Poirier, T. M. Dawson, and V. L. Dawson.** 2006. Apoptosis-inducing factor mediates poly(ADP-ribose) (PAR) polymer-induced cell death. Proc. Natl. Acad. Sci. USA **103:**18314–18319.
85. **Yu, S. W., H. Wang, M. F. Poitras, C. Coombs, W. J. Bowers, H. J. Federoff, G. G. Poirier, T. M. Dawson, and V. L. Dawson.** 2002. Mediation of poly-(ADP-ribose) polymerase-1-dependent cell death by apoptosis-inducing factor. Science **297:**259–263.
86. **Yuste, V. J., R. S. Moubarak, C. Delettre, M. Bras, P. Sancho, N. Robert, J. d'Alayer, and S. A. Susin.** 2005. Cysteine protease inhibition prevents mitochondrial apoptosis-inducing factor (AIF) release. Cell Death Differ. **12:**1445–1448.
87. **Yuste, V. J., I. Sanchez-Lopez, C. Sole, R. S. Moubarak, J. R. Bayascas, X. Dolcet, M. Encinas, S. A. Susin, and J. X. Comella.** 2005. The contribution of apoptosis-inducing factor, caspase-activated DNase, and inhibitor of caspase-activated DNase to the nuclear phenotype and DNA. J. Biol. Chem. **280:**35670–35683.
88. **Zong, W. X., D. Ditsworth, D. E. Bauer, Z. Q. Wang, and C. B. Thompson.** 2004. Alkylating DNA damage stimulates a regulated form of necrotic cell death. Genes Dev. **18:**1272–1282.
89. **Zong, W. X., and C. B. Thompson.** 2006. Necrotic death as a cell fate. Genes Dev. **20:**1–15.
90. **Zornig, M., A. Hueber, W. Baum, and G. Evan.** 2001. Apoptosis regulators and their role in tumorigenesis. Biochim. Biophys. Acta **1551:**F1–F37.